Journal of Sea Research 202 (2024) 102543

Contents lists available at ScienceDirect

Journal of Sea Research

journal homepage: www.elsevier.com/locate/seares

Dynamic of upwelling variability in southern Indonesia region revealed from satellite data: Role of ENSO and IOD

Herlambang Aulia Rachman [a,*], Martiwi Diah Setiawati [b,c,*], Zainul Hidayah [a], Achmad Fachruddin Syah [a], Muhammad Rizki Nandika [b], Jonson Lumban-Gaol [d], Abd. Rahman As-syakur [e], Fadli Syamsudin [f]

[a] Department of Marine Sciences and Fisheries, Faculty of Agriculture, University of Trunojoyo Madura, Jalan Raya Telang No 02, Kamal- Bangkalan, East Java 69162, Indonesia
[b] Research Center for Oceanography, National Research and Innovation Agency (BRIN), Jakarta, Indonesia
[c] Institute for the Advanced Study of Sustainability (UNU-IAS), United Nations University, Jingumae 5-53-70, Shibuya-ku, Tokyo 1508925, Japan
[d] Department of Marine Science and Technology, Faculty of Fisheries and Marine Science, Bogor Agricultural University, Bogor 16680, Indonesia
[e] Marine Science Department, Faculty of Marine and Fisheries, Udayana University, Bukit Jimbaran Campus, Bali 80361, Indonesia
[f] Study Center of Climate and Regional Maritime Management, Faculty of Fisheries and Marine Sciences, Universitas Padjadjaran, Jalan Raya Bandung-Sumedang KM 21 Jatinangor West Java 45363 Indonesia

ARTICLE INFO

Keywords:
Satellite data
Upwelling
Southern Indonesia
Correlation
El Niño Southern Oscillation (ENSO)
Indian Ocean Dipole (IOD)

ABSTRACT

The Southern Indonesian (SI) region is known for its high-intensity coastal upwelling caused by monsoonal wind. Interannual phenomena such as El Niño Southern Oscillation (ENSO) and Indian Ocean Dipole (IOD) also influence upwelling activity in this region. This study analyzed the relationship between upwelling intensity (UI_{sst}) and those variables and their impact on oceanographic features such as Sea Surface Temperature (SST) and chlorophyll-a concentration. We used satellite imagery data, including SST from the National Oceanic and Atmospheric Administration (NOAA) and chlorophyll-a from MODIS, to analyze the aforementioned issue. To identify the impact of wind patterns on coastal upwelling, we analyzed using zonal wind stress from ERA-5 Data. Quantification of UI_{sst} is defined as the SST gradient between the coastal and open ocean waters. Linear and partial correlation analysis between UI_{sst} with the Ocean Niño Index (ONI) and Dipole Mode Index (DMI) were conducted to see the influence of ENSO and IOD phenomena. Anomaly analysis was also conducted on SST, chlorophyll-a concentration, zonal windstress and UI_{sst} to see how large the values were during the years of the ENSO and IOD events. Upwelling in the SI region typically occurs during southeast monsoon (SEM) periods, starting earlier in the East side (Nusa Tenggara Islands) and moving towards the West side (South Coast of Java). The correlation analysis (both linear and partial) indicates that the IOD has a stronger influence on UI_{sst} in the SI region compared to ENSO, especially during June to October (SEM periods). This finding is confirmed by anomaly analysis, which reveals significant changes in SST, chlorophyll-a concentration, zonal windstress, and UI_{sst} during ENSO and IOD events. The magnitude of the anomalies is generally stronger during IOD events than those observed under ENSO conditions.

1. Introduction

Upwelling is one of the most significant physical processes for primary production. The process lifted the water from the deeper to the surface layer, bringing cold water rich in nutrients. This phenomenon is generally characterized by a decline in sea surface temperature (SST) and a rise in salinity and chlorophyll-a concentration (Setiawan et al., 2019; Wirasatriya et al., 2020; Xu et al., 2021). By modulating the amount, composition, and structure of phytoplankton, this phenomenon affects the operational dynamics of marine ecosystems, impacting the nutrient cycle, overarching productivity, and carbon release. Consequently, they give rise to some of the most prolific fishing grounds globally. Within maritime domains, the investigation into the extensive repercussions of upwelling transcends the fisheries domain and encompasses broader considerations, including marine conservation, climate changes, the foundational underpinning of food availability,

* Corresponding Authors.
E-mail addresses: herlambangauliarachman@gmail.com (H.A. Rachman), martiwi1802@gmail.com (M.D. Setiawati).

https://doi.org/10.1016/j.seares.2024.102543
Received 28 April 2024; Received in revised form 11 August 2024; Accepted 11 September 2024
Available online 12 September 2024

ecosystem management, and the economic prosperity of these regions (Hein et al., 2013; Undap et al., 2023).

In Indonesia, upwelling is predominantly caused by monsoon winds, specifically the southeast monsoon (SEM), although several upwelling phenomena also occur during northwest monsoon (NWM) (Wirasatriya et al., 2021). The SEM upwelling phenomena are typically more powerful and widespread (Purba and Khan, 2019). Several Indonesian regions have recorded upwelling phenomena, such as West Sumatera, South Bali-Nusa Tenggara, Flores, Banda, and Arafura Sea (Horhoruw et al., 2017; Ningsih et al., 2013; Wirasatriya et al., 2020). In particular, the southern part of Indonesia is the only example area where eastern border upwelling occurs in the Indian Ocean during SEM (Vinayachandran et al., 2021), and this is related to the South Java Current's reversal (Susanto et al., 2001). Therefore, these areas were observed to have high nutrients, high concentration of chlorophyll-a, high primary productivity, lowered water clarity, or caused low-oxygen issues (Horii et al., 2023; Vinayachandran et al., 2021; Wen et al., 2023). Based on the satellite dataset, high chlorophyll- a (higher 2 mg/m^3) is initially observed off Java in June and lasts until November, with the highest primary productivity above 1 $mgC/m^2/d$ (Hood et al., 2017). Moreover, during the upwelling, zooplankton biomass increases seasonally (Vinayachandran et al., 2021). However, downwelling Kelvin waves and weakened SEM winds suppress productivity during the transition period from NWM to SEM (Sprintall et al., 1999). The upwelling also has indirect impacts, such as excessive jellyfish or hazardous algal bloom seasons (Wahyudi et al., 2023), as well as notable alterations to the coastal ecosystems. Moreover, the Southern Indonesian (SI) region (i.e., South Java, South Bali-Nusa Tenggara) is known as the location with high productivity of economic fish such as tuna and other small pelagic fishes (Lumban-Gaol et al., 2015; Setiawati et al., 2024; Yati et al., 2024).

Prior investigations have shown that the SI region is influenced by several variables on regional, local, and global scales such as Monsoon, El Niño Southern Oscillation (ENSO) (Rachman et al., 2020; Susanto et al., 2001), and Indian Ocean Dipole (IOD) (Horii et al., 2018; Lumban-Gaol et al., 2021). The SI region is highly correlated with ENSO and IOD, especially during SEM periods (As-syakur Abd et al., 2014). This period is the peak of the upwelling event in the SI region. In addition, this area is also an outflow region of the Indonesian Throughflow (ITF), a current that flows from the Pacific to the Indian Ocean. The warmer water from the ITF current also impacts the variability of upwelling intensity (Susanto et al., 2001).

The high intensity of upwelling is an important indicator of ocean productivity and fishing ground area. The SI region is well known for producing many varieties of highly valuable tuna (Setiawati et al., 2015; Syah et al., 2019; Syamsuddin et al., 2016). Also, some studies mention that the abundant of tuna production occurred during SEM periods (Lumban-Gaol et al., 2015; Nugroho et al., 2023; Sambah et al., 2017; Setiawati et al., 2024). In addition, the SI region is also known as one of the migration sites of several types of marine megafauna, such as cetaceans and mantas (Sahri et al., 2021). Therefore, understanding the intensity of upwelling is crucial for this region, as it is linked to its economic benefits, such as fisheries productivity. The Upwelling Index (UI) is a common method used to determine the intensity of upwelling (e.g., Benazzouz et al., 2014; Jacox et al., 2018). Several UI's have been employed to assess upwelling intensity in this area, including wind-based UI, SST-based UI (UI_{sst}), and Chlorophyll-based UI (e.g., Budiman et al., 2022; Wen et al., 2023). According to Budiman et al. (2022), the SST-based UI is particularly more effective in identifying upwelling intensity in this region, as it exhibits a shorter time lag compared to other UI's when chlorophyll-a levels increase.

Previously, numerous researchers have conducted studies on upwelling in the SI region, utilizing both field observation data and remote sensing data and models. Wyrtki (1962) was one of the early studies to identify upwelling events in this region. With advancements in remote sensing and modeling technology, subsequent researchers, including by Ningsih et al. (2013), Susanto et al. (2001, 2006), and Wirasatriya et al. (2020), further explored the spatial and temporal distribution of upwelling in the study area. Additionally, previous analyses have examined the connection between upwelling anomalies with ENSO and IOD. For instance, Susanto and Marra (2005), investigated the impact of the 1997/98 El Niño on chlorophyll-a variability. While Wen et al. (2023) explored the influence of ENSO and IOD on upwelling patterns. Generally, these studies indicate that the upwelling in SI is seasonal and occurs during the SEM season as well as influenced by ENSO or IOD. However, these studies often lack comprehensive information, such as Susanto and Marra (2005), which only analyzed the role of ENSO on upwelling conditions, or Wen et al. (2023), which analyzed upwelling anomalies only during ENSO and IOD events, with separate analysis, without determining which phenomenon had the most influence. Therefore, it is essential to conduct a more comprehensive analysis of the long-term variability of upwelling in the SI region and simultaneously examine the influence of ENSO and IOD to understand the independent spatial-temporal effects of these phenomena on upwelling. This comprehensive analysis has not been performed by previous researchers. Therefore, this study, it is hoped, can provide more comprehensive insights into upwelling variability and its connection to global phenomena.

Remote sensing technology is one of the methods that can be used to observe some oceanographic parameters such as SST, chlorophyll-a, and sea wind. The availability of remote sensing data for observation of oceanographic parameters is currently long enough (more than 30 years) for several datasets. In these studies, we analyzed the long-term variability of upwelling intensity and oceanographic features based on remote sensing data from 1982 to 2022. Moreover, we analyzed the impact of the ENSO phenomenon on the anomalies of upwelling intensity, SST, chlorophyll-a concentration, and zonal windstress in the SI region. To understand the influence of ENSO and IOD on upwelling, we also conducted both linear and partial correlation analysis. The findings of this research aim to offer more comprehensive insight into the upwelling phenomena in the SI region and its association with global climate phenomena such as ENSO and IOD.

2. Data and method

2.1. Study area

This research was carried out in the SI waters stretching from the South Coast of Java to the South Coast of Nusa Tenggara with coordinates of 6°S to 15°S latitude and 106°E to 125°E longitude (Fig. 1). This region is known to have a high intensity of upwelling and becomes the outlet of the ITF through the Lombok Strait and Ombai Strait. The lines in Fig. 1 are locations that represent coastal and ocean areas in the process of calculating the upwelling index value.

2.2. Data

To identify the magnitude of upwelling, we used SST data derived from the Optimum Interpolation Sea Surface Temperature (OISST) ¾ developed by the National Oceanic and Atmospheric Administration (NOAA) for 1982–2022. This data has a daily temporal resolution and spatial resolution of 0.25 degrees. This data results from a combination of satellite data, field surveys, and ship buoys, which are then assimilated to produce regular gridded data. This data can be downloaded using the following link: https://psl.noaa.gov/data/gridded/data.noaa.oisst.v2.html. More detailed information on the data can be found in (Reynolds, 2009). To understand the impact of the high intensity of upwelling, we identified it with chlorophyll-a concentration data obtained from level 3 data of the Aqua Moderate Resolution Imaging Spectroradiometer (MODIS). It has a spatial resolution of 4 km and is recorded monthly. In this study, the data used is from 2002 to 2022. The data can be accessed at https://oceancolor.gsfc.nasa.gov/l3/. The wind speed data was obtained from the ECMWF Reanalysis (ERA 5) archives

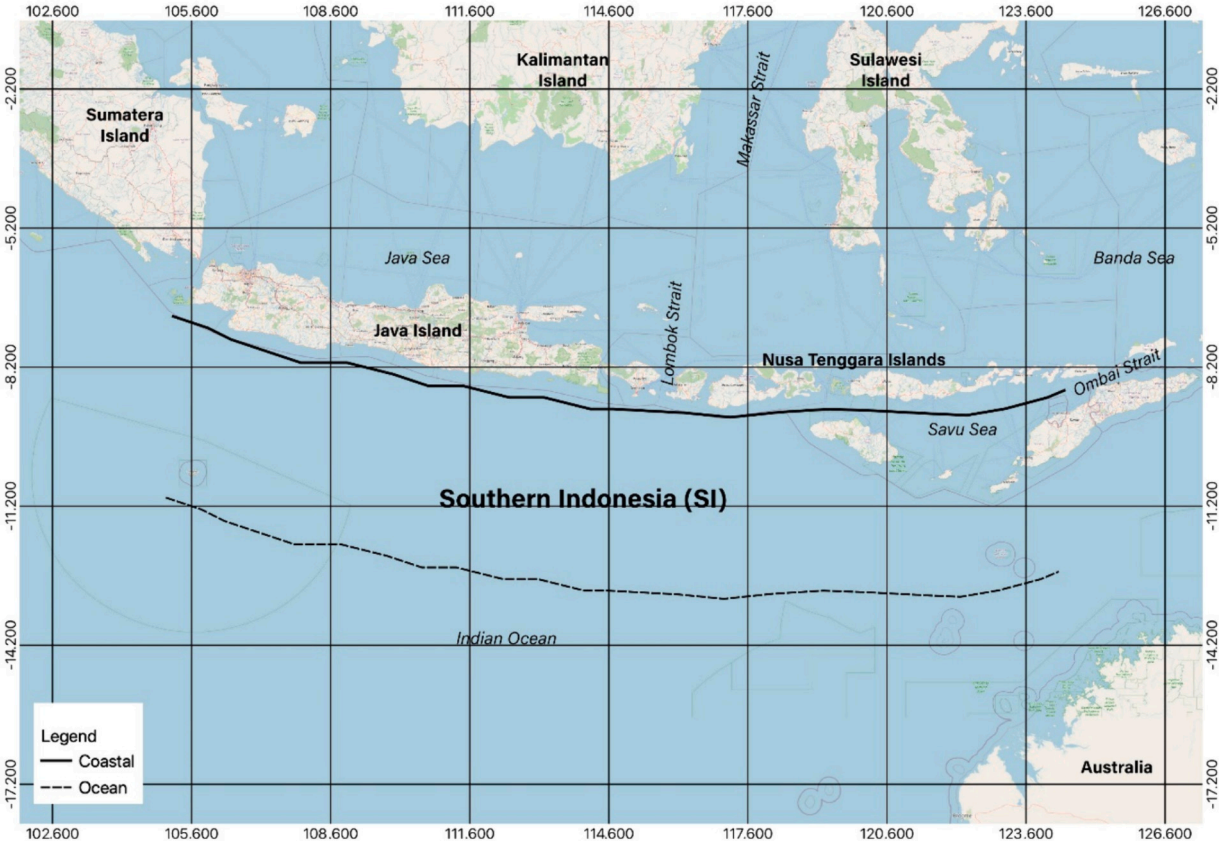

Fig. 1. The study area at the Southern Indonesia (SI) Seas. The bold and dashed line indicates the coastal-ocean line transect used to calculate the upwelling index.

with a spatial resolution of 0.25° x 0.25° at regular intervals (monthly dataset from 1982 to 2022). It has been found to be well-aligned and suitable for analyzing wind stress and curl in order to assess upwelling intensities (Jayaram and Jose, 2022). The data can be obtained at https://cds.climate.copernicus.eu/cdsapp#!/dataset/reanalysis-era5-single-levels-monthly-means?tab=overview.

In this study, the dynamics of upwelling conditions were examined in relationship with interannual phenomena such as the ENSO and IOD. For the year of the ENSO phenomenon, data from the Ocean Niño Index (ONI) was used, which can be accessed at https://origin.cpc.ncep.noaa.gov/products/analysis_monitoring/ensostuff/ONI_v5.php. ONI data describes the value of Sea Surface Temperature Anomaly (SSTA) found in the Niño 3.4 region. Next, for the IOD phenomenon, the period of the event year was determined based on the value of Dipole Mode Index (DMI) data obtained from http://www.jamstec.go.jp/aplinfo/sintexf/DATA/dmi.monthly.txt. The year of occurrence of each phenomenon can be seen in Table 1. The anomaly values of SST, chlorophyll-a, and windstress will be calculated in each extreme phenomenon condition.

Table 1
Year of Occurrence: the ENSO and IOD event based on ONI and DMI data.

Phenomenon			
El Niño	La Niña	Negative IOD	Positive IOD
1982	1983	1984	1982
1986	1988	1985	1994
1987	1995	1989	1997
1991	1999	1996	2006
1994	2000	1998	2007
1997	2005	2010	2008
2002	2007	2013	2011
2004	2008	2016	2012
2006	2010	2020	2015
2009	2011	2021	2019
2014	2016	2022	
2015	2017		
2018	2020		
	2021		
	2022		

2.3. Method

2.3.1. Upwelling index

One characteristic of strengthening upwelling intensity is decreased SST in coastal areas. To quantify upwelling intensity in the SI region, we perform the Upwelling Indices based on SST data (UI_{sst}), which means the gradient between SST in coastal and ocean areas. The calculation of this index follows this equation:

$$UI_{sst} = SST_{ocean} - SST_{coast} \quad (1)$$

The SST dataset was extracted by line transect that represents the coastal and ocean location (Fig. 1). The positive value of UI_{sst} means the desirable upwelling condition, and vice versa, while a negative value.

Upwelling is a phenomenon that occurs due to forcing from wind forces aligning with the coastline, resulting in windstress that generates Ekman currents. To clarify the wind strength of this occurrence, it is analyzed based on the value of windstress. In this study, wind strength is represented in the form of zonal windstress which is the strongest component of wind friction that generates upwelling in the southern waters of Indonesia (Siswanto and Suratno, 2005; Susanto et al., 2006). The equation used in calculating the zonal windstress component is as follows:

$$\tau_x = \rho_a C_d U^2 U_{10} \quad (2)$$

Where ρ_a is the air density (1.25 kg m^{-3}), C_d is the drag coefficient (2.6×10^{-3}), U^2 is the magnitude of windspeed, and U_{10} is the zonal

wind component. The magnitude of windspeed is calculated based on the zonal (U_{10}) and meridional (V_{10}) components of the ERA-5 data.

2.3.2. Anomaly and correlation analysis

Analysis of monthly climatology was carried out to understand the monthly variations of upwelling intensity and other oceanographic features in SI regions. The climatological average following for the equations:

$$\overline{X} = \frac{1}{n}\sum_{i=1}^{n} xi(x,y,t) \tag{3}$$

Where the $\overline{X}$ is the monthly climatology value at (x,y) locations, xi(x, y,t) is the i-th value of data at (x,y) and time (t), and n is the number of monthly data in one period of climatology. We used the anomaly analysis to understand the deviations of each parameter during the ENSO and IOD years. Where there is a deviation of data during the i-th month with monthly climatology data.

To analyze the influence of the interannual variability of the ENSO and IOD, we used the linear and partial correlation between UI_{sst} with ENSO and IOD indices, which are represented by ONI and DMI, respectively. Partial correlation is employed to quantify the relationship between two variables that are related while accounting for the influence of one or more additional variables or assuming that these variables remain constant (Blair, 1918). As previously described, the southern region of Indonesia is affected by ENSO and IOD. However, it is essential to identify which regions and at what times are significantly influenced by ENSO or IOD. In this context, the partial correlation will examine the strength of the relationship between UI_{sst} and ONI while treating the third variable, DMI, as constant and conversely for ONI. Previously, partial correlation analysis has been applied to investigate the effects of ENSO and IOD events on rainfall and SST (e.g., Ashok et al., 2007). Therefore, a partial correlation analysis was conducted to see the effect of each parameter independently (As-syakur Abd et al., 2014). The partial correlation equation used is as follows:

$$R_{par} = \frac{r_{12} - r_{13}r_{23}}{\sqrt{(1-r_{13}^2)(1-r_{23}^2)}} \tag{4}$$

Where R_{par} is a partial correlation between two variables (1 and 2) by eliminating other variables, 3. This study conducted a partial correlation analysis between UI_{sst} with ONI and DMI. When correlating with ONI, the effect of DMI will be eliminated and vice versa. For example, if we want to do a partial correlation (R_{par}) between UI_{sst} and ONI, r_{12} is the correlation between UI_{sst} and ONI, r_{13} is UI_{sst} with DMI, and r_{23} is ONI with DMI. The result of this calculation will explain how much influence each has on the intensity of Upwelling in the SI region. Confidence levels of 95 % are used to determine the significance level of correlation.

3. Result

3.1. Monthly variation

We analyzed the monthly climatology of SST, chlorophyll-a, and zonal wind stress along the SI region from January to December over the periods of each dataset. The monthly climatology analysis shows that there is a spatiotemporal variation of each variable. Figs. 2, 3, and 4 show the monthly climatology of SST, chlorophyll-a concentration, and zonal wind stress in the SI region based on periods of each dataset. The dynamics of SST value are observed starting in May, particularly in the Southern Region of Nusa Tenggara Islands, with a range between 25 and 26 °C. The decrease in SST began to extend westward in the South Coast of the Java Region by reaching its lowest point during the August – September period, where the SST range was at 24–26 °C. Next, in the October – December period, the SST value increased again up to 30 °C, where the southern part of East Nusa Tenggara started to increase first

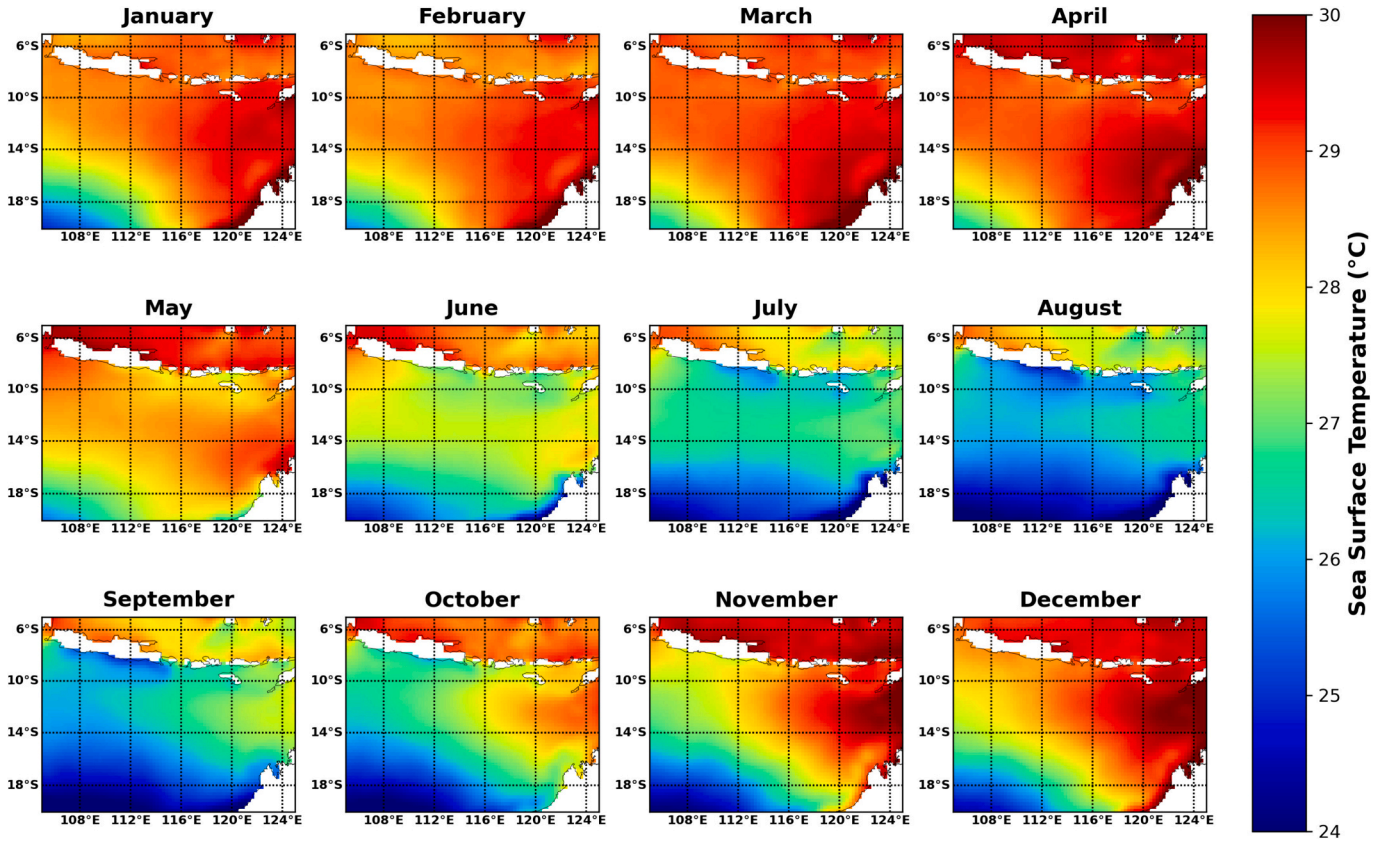

Fig. 2. Monthly Climatology of SST in the South Indonesian Region.

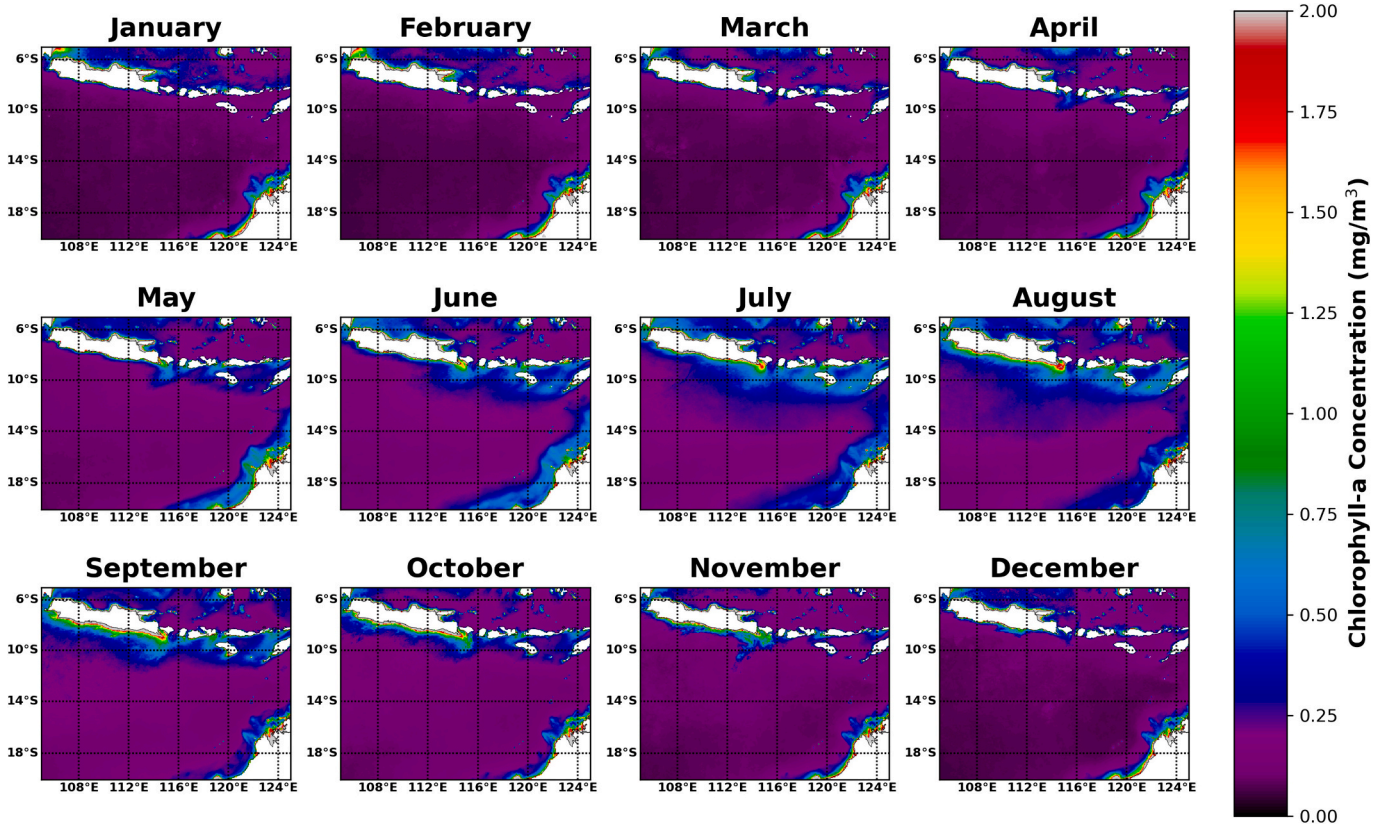

Fig. 3. Monthly Climatology of Chlorophyll-a Concentration in SI Region.

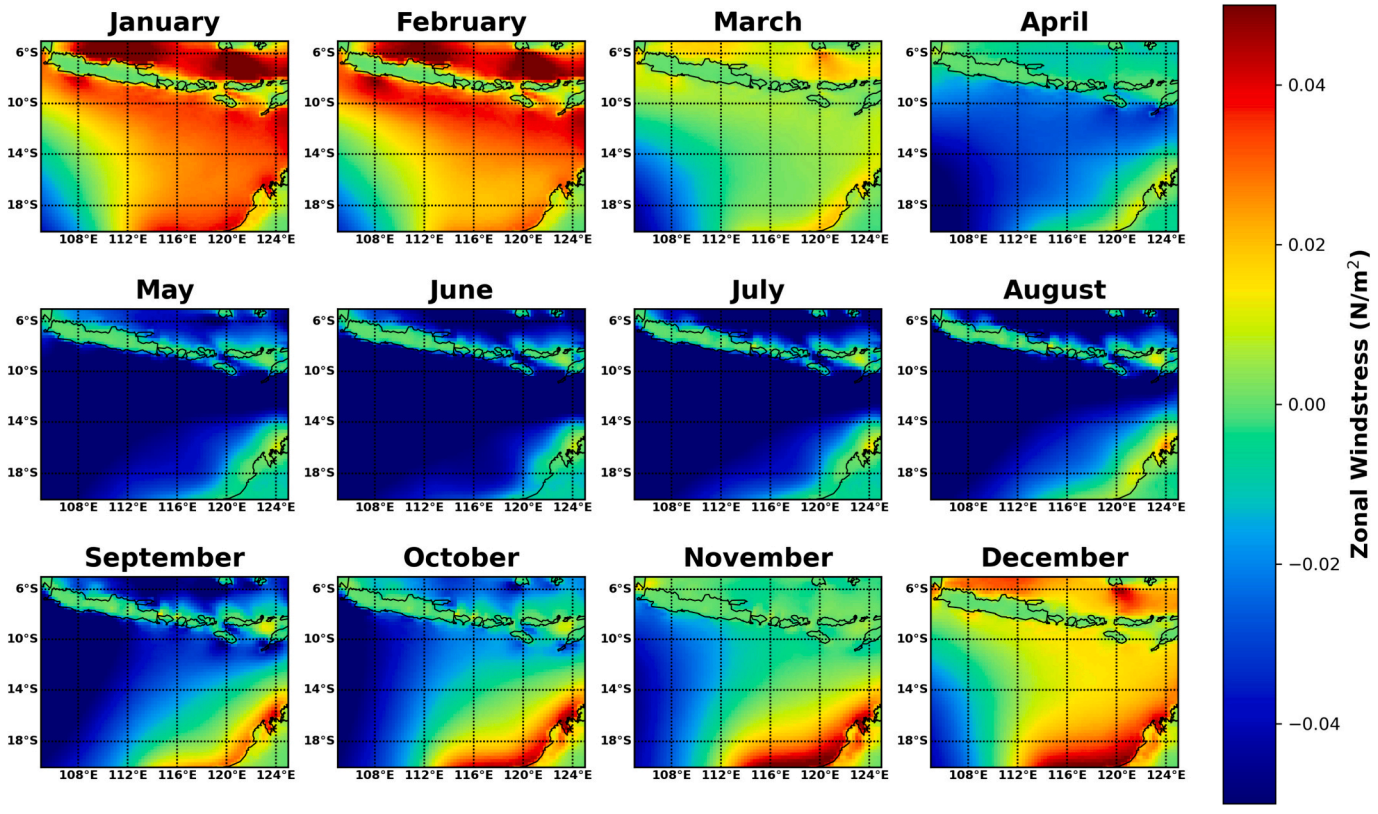

Fig. 4. Monthly Climatology of Zonal Windstress in SI Region.

and then moved towards the western region on the South Coast of Java. During the period from January to March, the distribution of SST tends to exhibit elevated value, exceeding 30 °C across the SI region. Based on these results, it can be inferred that the pattern of SST changes seasonally. The SEM period is typically associated with lower SST, while NWM periods are characterized by warmer SST.

To quantify the effect of upwelling, we also performed a monthly average analysis of chlorophyll-a concentration. The finding reveals that monthly variation changes in chlorophyll-a concentration align with the SST pattern. The chlorophyll-a concentration tends to be higher from June to November (SEM) than from December to May (NWM). The increases in chlorophyll-a concentration began to appear from May to June, especially on the Southern part of Nusa Tenggara Islands, with concentrations ranging from 0.77 to 1.50 (mg/m^3). The same pattern is seen with the decrease in SST, where the increase in chlorophyll-a concentration also moves westward from the August to September period. The peak of the highest chlorophyll-a concentration occurred in September and reached 2.5 mg/m^3 along the SI region (South Coast of Java and Bali-Nusa Tenggara Islands). This phenomenon was related to the increasing upwelling intensity in SI regions.

Fig. 4 depicts the monthly variation of zonal windstress from 1982 to 2022. Positive (negative) values of windstress illustrate westward (eastward) directions of the zonal wind stress. According to the figure, the SI region experienced negative wind stress curl from May to October (SEM), with the highest wind stress magnitude of -0.05 N/m^2, while positive wind stress curl occurred from December to February (NWM). The SEM condition is characterized by stronger wind stress patterns moving from east to west, which corresponds to a period of high upwelling intensity marked by a decrease in temperature and an increase in chlorophyll-a concentration. Conversely, during the NWM period, wind stress tends to be positive, moving eastward. This results in lower upwelling intensity during this period.

One of the characteristics of the upwelling phenomena is the decrease of SST in coastal areas. To quantify the upwelling strength of this study, it was performed by calculating the gradient between the SST on the coast and ocean location. The UI_{sst} results indicate a temporal difference in occurrence between the western region (south of Java) and the eastern region (south of Nusa Tenggara). In the eastern region, high UI_{sst} values are observed from March to June (hotspot peak in May), whereas in the western region, they occur from June to November (hotspot peak values during July to September). It shows that the upwelling phenomena begin to form in the eastern region between 120 and 122°E during the April – May period in the Southern part of Timor Island, East Nusa Tenggara. In the west region of SI, the increase in the UI_{sst} began in the South Coast of Java (106–114°E) during the June – July period, when the UI_{sst} reached 0.4 °C. The peak of upwelling phenomena occurred from August to September, with the UI_{sst} reaching 0.9 °C along the southern part of Central and West Java Province (112–114°E). The region between 116°E and 118°E exhibits relatively low UI_{sst} values, peaking at only 0.1 °C from May to November. In contrast, the UI_{sst} values in the western and eastern regions remain significantly higher during the same period. This area, situated just south of the Lombok Strait and Alas Strait, serves as the outlet for the ITF current. During the west monsoon season, UI_{sst} values in this region tend to rise, reaching up to 0.4 °C. The low intensity of UI_{sst} is further supported by the relatively low concentrations of chlorophyll-a observed in the same period and location.

3.2. Partial correlation

Fig. 6 shows a correlation analysis to see the influence of the ENSO and IOD phenomena on the intensity of upwelling in the Southern Indonesian Sea. The analysis used correlation and partial correlation methods between UI_{sst}, ONI, and DMI indices. Partial correlation was carried out to describe the phenomenon's effect more clearly by eliminating the influence of the impact of other phenomena. The results of the correlation between UI_{sst} and ENSO show that the influence of the ENSO phenomenon is significant from June to December, with a value above 0.3. The influence of the ENSO phenomenon peaks in the October to December period in the southern region of Java with a correlation of 0.5. Whereas for the eastern part (South Bali Nusa Tenggara), the highest correlation occurs in the April to July period in the southern part of Flores Island to the Sabu Sea. The ENSO influence was relatively low from October to December in the eastern part. The next result is the correlation between IOD and UI_{sst}, where the results are quite high, especially in the Southeast Monsoon period (June–November) in the South of Java (105–115°E). The peak correlation coefficient occurred in the August–September period, reaching 0.7 in the southern waters of West Java (longitude 106–108°E) and the southern part of East Java (longitudes 112–114°E). Whereas for the southern region of Bali-Nusa Tenggara, the effect is fairly high only in the southern region of Sumbawa Island (Longitude 116–120°E) from June to August. Besides these periods, the influence of the IOD phenomenon on the strength of UI_{sst} tends to have no significant correlation. While a notable phenomenon is observed in the region of longitude 117°E, which is one of the exit points of ITF, the low correlation between UI_{sst} with both ENSO and IOD, which generally remains below 0.3 for almost the entire year.

A partial correlation analysis method was performed to observe a clearer effect of both phenomena (ENSO and IOD) on upwelling intensity. With this method, the effect of a phenomenon can be seen by eliminating the impact of other phenomena. The results of partial correlation with the ENSO phenomenon after removing the impact of IOD show that the most significant influence occurs in the southern region of Java in the period of November, with a coefficient value reaching more than 0.6 (Fig. 5). Meanwhile, the influence of ENSO observed in the linear correlation in the same region from May to October has weakened when partial correlation is applied, indicating that the region is actually influenced by IOD, as seen in Fig. 6 (bottom right). For the South Bali-Nusa Tenggara region (Longitude 116–120°E), the results also show that the influence of ENSO is significant in the April to May period, with a partial correlation coefficient reaching 0.3, where the Hovmoller diagrams indicate a relatively similar pattern to the linear correlation. However, there is a slight variation, particularly in June, in which the distribution is indicated to be influenced by the Indian Ocean Dipole (IOD). In contrast, the partial correlation between UI_{sst} and IOD after removing the effect of ENSO shows a strong coefficient (>0.3) from May to October along the southern coast of Java and is relatively like its linear correlation, indicating that this area is not influenced by ENSO. For the Southern Bali-Nusra Southern Waters, the high influence of IOD only occurs in the southern part of Sumbawa and Flores Island from June to September. In this region, the influence of the ENSO and IOD phenomena appears to be more complex, with a heterogeneous distribution of influence. While ENSO has a significant impact during April–May and a smaller influence in July, IOD is seen to have an impact from June to October, although this is not observed throughout the entire eastern region.

3.3. Anomaly condition

An anomaly is a difference in general conditions at a certain time. This study analyzed anomalies to determine the value of upwelling intensity, SST, and chlorophyll-a during extreme conditions (ENSO and IOD). The previous analysis revealed that the intensity of upwelling in the SI region strongly correlates with the ENSO and IOD phenomena. The monthly anomaly analysis focuses on the periods from June to November, corresponding to the peak of upwelling in the SI region.

3.3.1. Upwelling index (UI_{sst}) anomaly

UI_{sst} anomaly analysis is calculated based on the difference between the UI_{sst} value in the extreme event years (Table 1) and the average condition. The results are displayed as a Hovmoller diagram showing the monthly pattern of ENSO or IOD evolution starting in the June–August

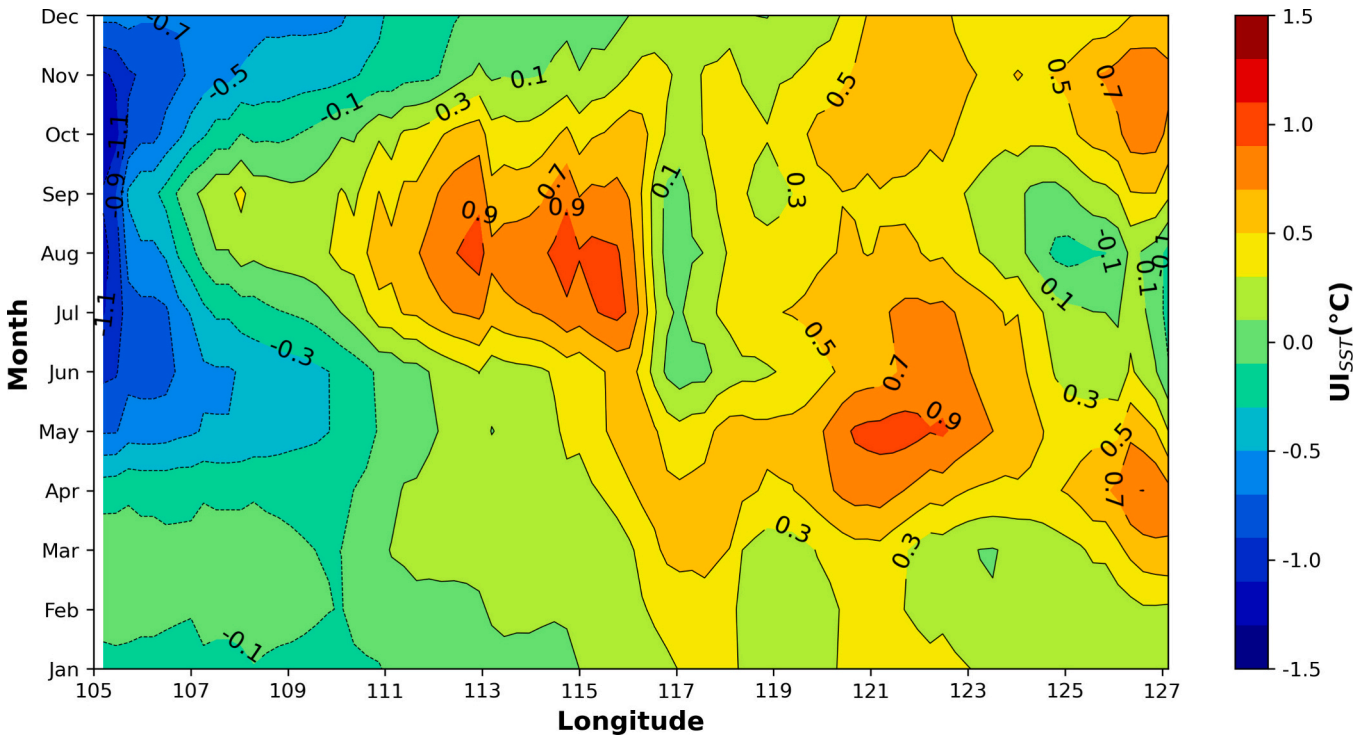

Fig. 5. Annual Cycle of Coastal Upwelling Index (UI_{sst}) in Southern Java-Nusa Tenggara.

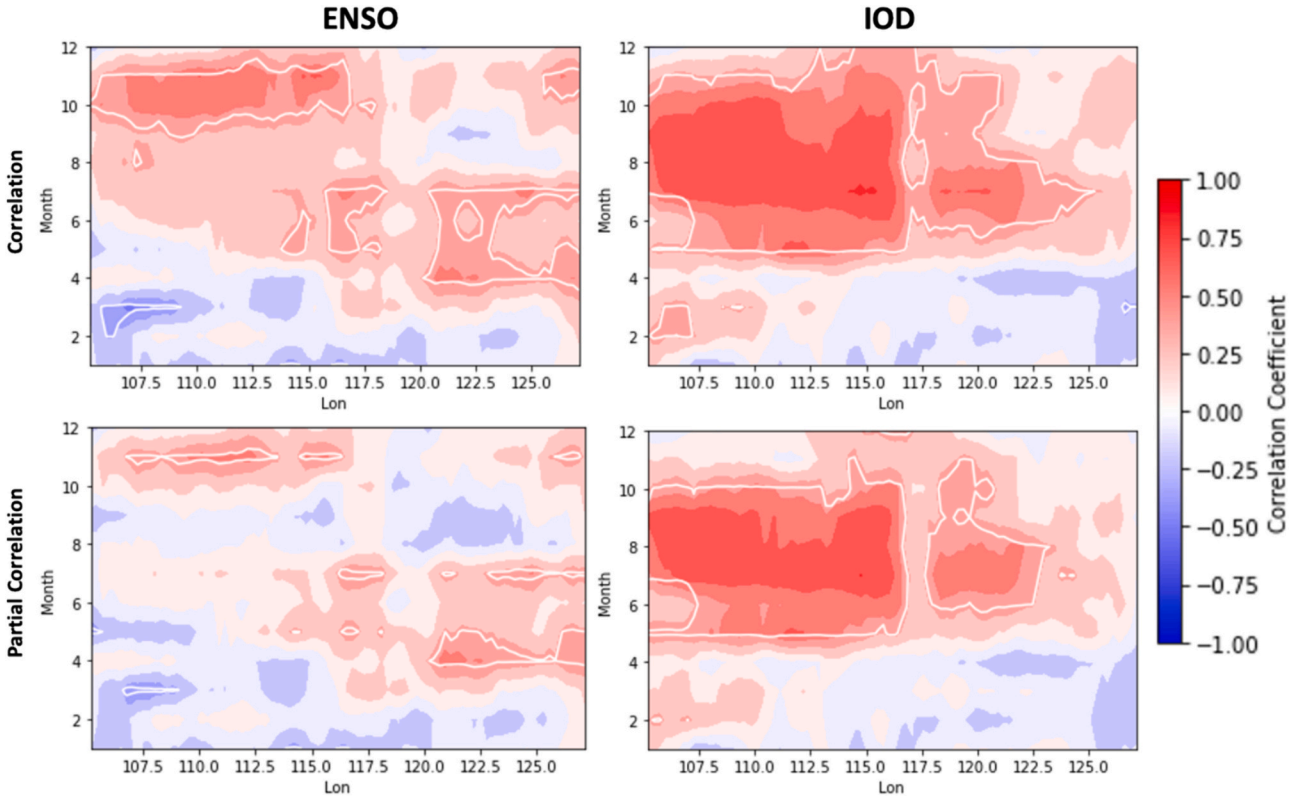

Fig. 6. The monthly partial/correlation between UI_{sst} with ENSO and IOD. The Y-ordinate indicates the month and the X-axis indicates the longitude. The white line indicates a correlation with 95 % significance.

period in the first year (0) and followed by January to May in the following year (1). The pattern is based on the evolution of ENSO and IOD, which begin to appear during the boreal summer, peak during the boreal winter, and begin to weaken during the spring of the following year (Juneng and Tangang, 2005; Saji et al., 1999). The results of the anomaly analysis show an increase (decrease) in the intensity of

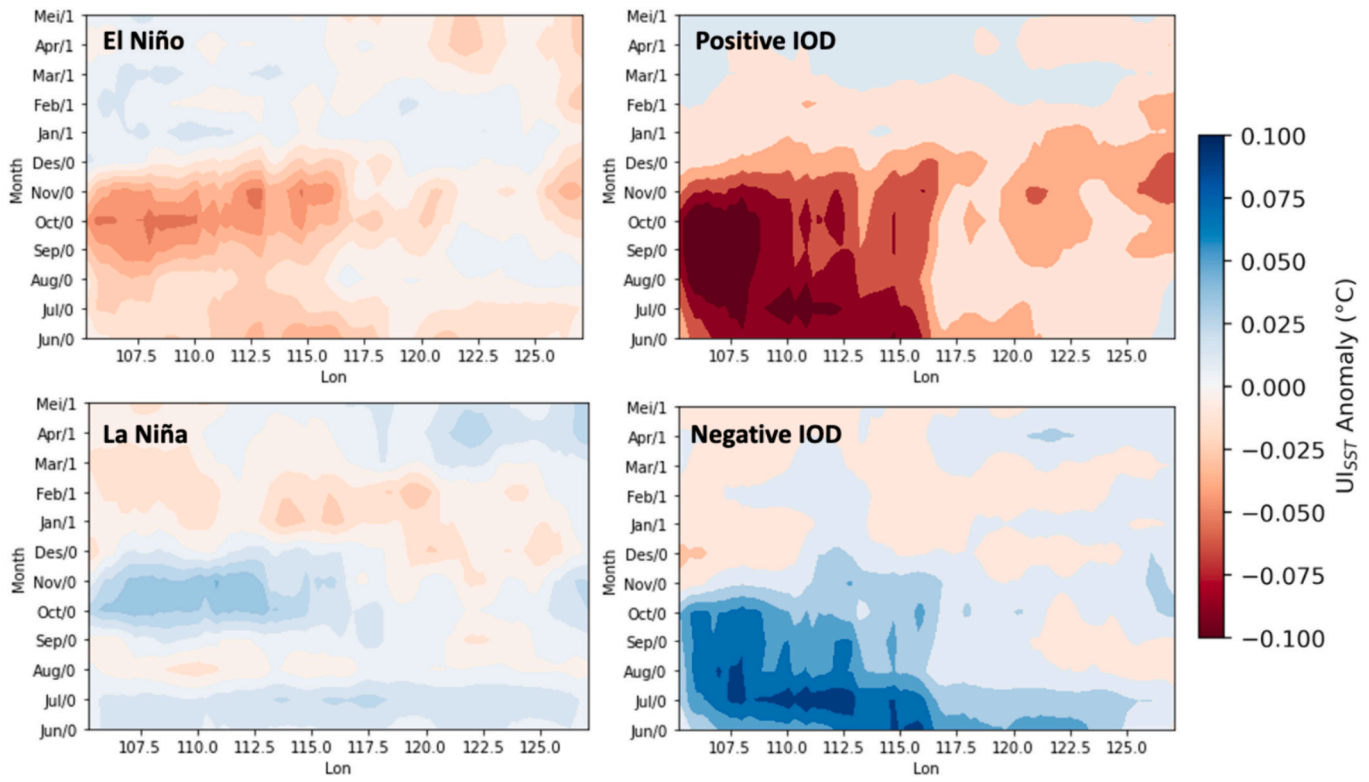

Fig. 7. Anomaly of Upwelling Index (UI_{sst}) during ENSO and IOD phenomena.

upwelling that occurs in each extreme condition, El Niño / Positive IOD (La Niña / Negative IOD) (Fig. 7). Under El Niño conditions, the intensity of upwelling in the SI region tends to experience positive anomalies in the August–November period, especially along the southern coast of Java. The maximum value of UI_{sst} Anomaly conditions during El Niño reached 0.5 in the southern waters of East Java Province. Meanwhile, the UI_{sst} anomaly value tends to be lower for the southern coastal region of Nusa Tenggara which is below 0.2. The opposite situation occurs during the La Niña phenomenon, where the value of UI_{sst} anomaly tends to be negative in the same period, especially along the southern coast of Java. The peak value of UI_{sst} anomaly during La Niña reached −0.4 in November around the south coast of Central Java Island.

IOD extreme conditions have a pattern that is not too different from ENSO but has a much stronger magnitude. This agrees with the results in Fig. 5, which show that UI_{sst} has a strong relationship with the IOD phenomenon. The high value of the positive (negative) anomaly of UI_{sst} when IOD phenomena generally occur in the period of June to November in the first year (0). The high anomaly did not increase until the following year (1). The peak of UI_{sst} anomaly conditions during Positive IOD occurs from June to November along the South coast of Java (105–116°S). The maximum anomaly value even reaches 1.4, especially on the southern coast of West Java Province (106–108°E in Longitudes). As for the southern coastal region of Nusa Tenggara, the UI_{sst} anomaly is quite high (reaching 0.7) around the southern waters of Flores Island (around the Sabu Sea). During the year of Negative IOD, the UI_{sst} anomaly pattern showed the opposite result during the same event period (June–November). Particularly on the South coast of Java, where the peak of UI_{sst} anomaly reaches −1.3 in Central Java and East Java. Meanwhile, for the Southern coastal region of Bali-Southeast Nusa Tenggara, the UI_{sst} anomaly reaches −0.5 and occurs only in June–July. These results prove that in the Positive (Negative) period, IOD causes an increase (decrease) of upwelling intensity.

3.3.2. *SST anomaly*

The results of the analysis for SST anomaly (SSTA) during extreme ENSO and IOD conditions are presented in Fig. 8. The SSTA value is focused on the peak period of the Upwelling phenomenon from June to November. Fig. 8 shows the pattern of SSTA in the SI region during ENSO events (El Niño and La Niña). In general, during El Niño (La Niña) conditions, the SSTA along the SI region tends to be lower (higher) than the average condition (monthly climatological value). The SSTA has a negative pattern from July to October, especially along the coast of Java Island. The peak of minimum value was observed in September with −0.54 °C in SSTA. On the southern part of Bali Nusa Tenggara, the SSTA pattern is also still negative, although not lower than on the southern coast of Java. During La Niña conditions, the opposite SSTA pattern is obtained, where SST values tend to be higher than in normal conditions (positive value). The SSTA value along the south coast of Java tends to be lower than the open ocean (far from the coastline). The highest pattern was found in locations far from the coastal area. The SSTA value in the coastal area reached the maximum value in October, which reached 0.4 °C.

The impact of the IOD phenomenon (Fig. 9) has the same pattern as ENSO, which causes anomalous values in SST conditions in the Southern Indonesian Waters. Based on the analysis results, SST anomaly values tend to be stronger than ENSO values during the IOD. Positive IOD conditions have the same pattern as the El Niño phenomenon, where negative anomalies occur along the southern coast of Indonesia. The negative SSTA conditions began in June, peaked in August, and reached −0.9 °C. The anomaly began to weaken in the October and disappeared in November. The spatial distribution shows that negative SSTA conditions mainly occur in the area along the South coast of Java. In the South Bali-Nusa Tenggara region, negative SSTA values tend to appear only from June to August with lower values (around −0.3 °C). Furthermore, when the IOD is negative, the pattern is similar to La Niña's. Where SSTA values tend to be positive, especially in areas along the southern coast of Java. The peak period of negative anomaly conditions in these locations occurs around June to September, which reaches 0.7 °C. During the

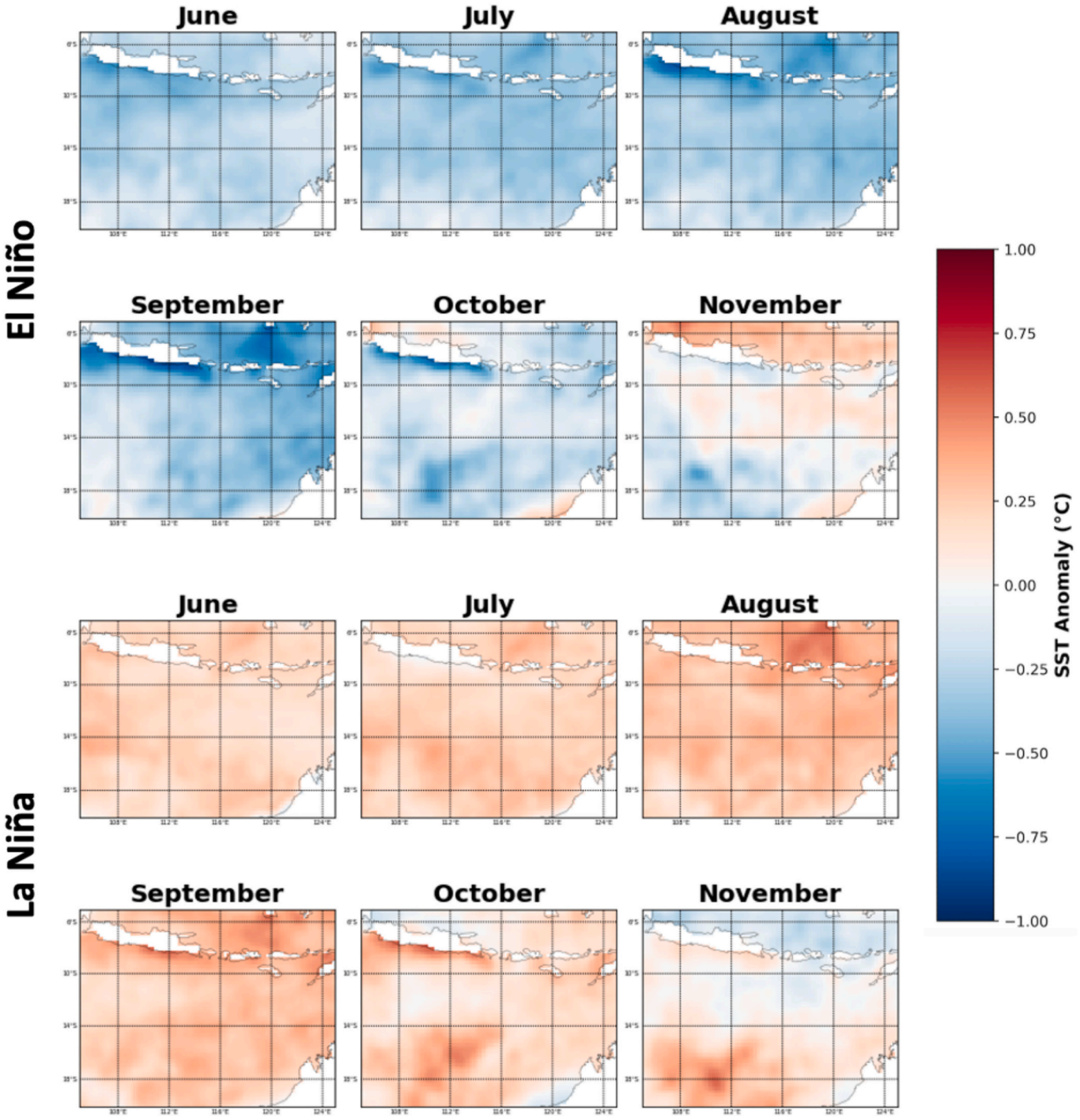

Fig. 8. SST Anomaly during El Niño and La Niña.

November period, the impact tends to begin to weaken and disappear.

3.3.3. CHL-a anomaly

Figs. 10 and 11 demonstrate the anomaly of chlorophyll-a concentration during ENSO and IOD conditions. The results of this analysis are used to confirm the increase (decrease) of upwelling intensity and SSTA anomaly under extreme conditions. During El Niño events, SST values along Java's south coast are lower than normal conditions. The Upwelling Index (UI) value during El Niño also exhibits anomalously positive (higher) values compared to normal conditions. Fig. 10 shows chlorophyll-a concentrations during El Niño are higher than normal (positive anomaly). In June, chlorophyll-a anomalies tend to occur in the southern region of East Java with an average value of 0.19 mg/mg^3. Furthermore, chlorophyll-a values tend to increase and peak in September, where positive anomalies dominate almost along the entire South coast of Java, Sumbawa Island, to the Sabu Sea region. The maximum anomaly of chlorophyll-a concentration in that period reached 0.27 mg/m^3 on the South coast of Java. In La Niña conditions, the chlorophyll-a anomaly has an opposite pattern compared to El Niño. Most of the southern waters of Java, Nusa Tenggara, and around the Sabu Sea experienced negative chlorophyll-a anomaly. The negative anomaly appeared in the July period in the East Java and Sabu Sea regions, then peaked in August–October. Current results also show that under La Niña conditions, the intensity of upwelling tends to decrease.

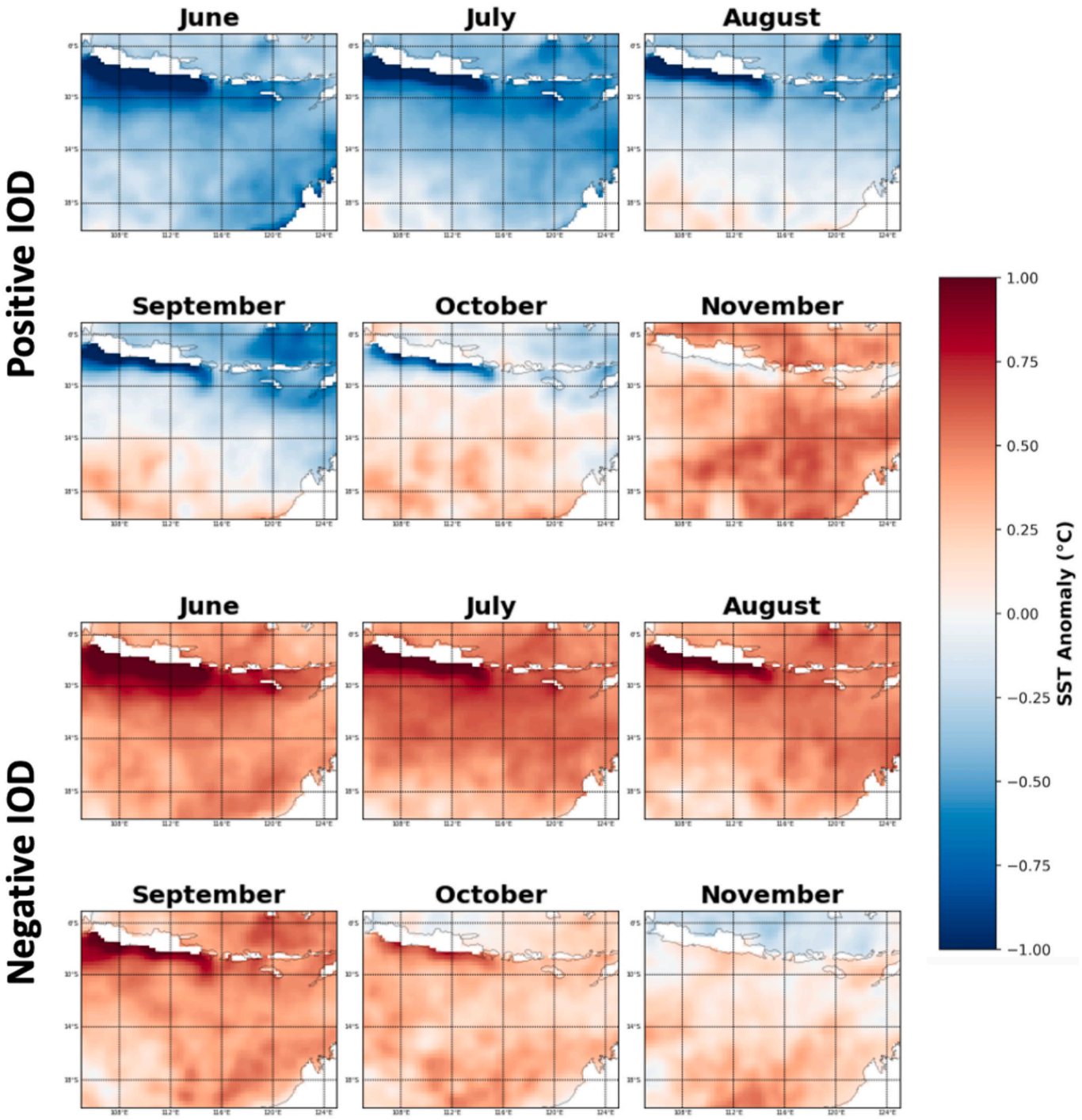

Fig. 9. SST Anomaly during Positive IOD and Negative IOD.

The magnitude of the chlorophyll-a anomaly in the peak period reached −0.16 mg/m^3.

The amplitude of positive anomalies in the Positive IOD phase has the same pattern as El Niño conditions, mostly occurring in South Java with larger values. The opposite condition occurs when the La Niña phenomenon and Negative IOD occur, with negative anomalous values for chlorophyll-a concentrations. Regarding amplitude value, the negative IOD phase tends to have a greater negative anomaly than La Niña conditions. The intensity of the rise in chlorophyll-a started to develop even in June and peaked in September. In this period, the chlorophyll-a anomaly reached 2.3 mg/m^3 with a distribution of almost all southern Indonesian waters (Java, Bali, to Nusa Tenggara). The high value of chlorophyll-a increase from the average condition is one of the reasons for the increase in fisheries productivity. Next, the Negative IOD shows the opposite pattern, where the chlorophyll-a anomaly tends to be negative with a stronger magnitude than La Niña. The peak period of negative IOD began in June and peaks in August and October. The lowest value of chlorophyll-a anomaly during negative IOD reached −1.8 mg/m^3. The high value of chlorophyll-a anomaly also confirms the previous analysis where UI_{sst} tends to have a stronger correlation to the IOD phenomenon.

3.3.4. *Windstress anomaly*

Figs. 12 and 13 show the windstress anomaly during the ENSO and

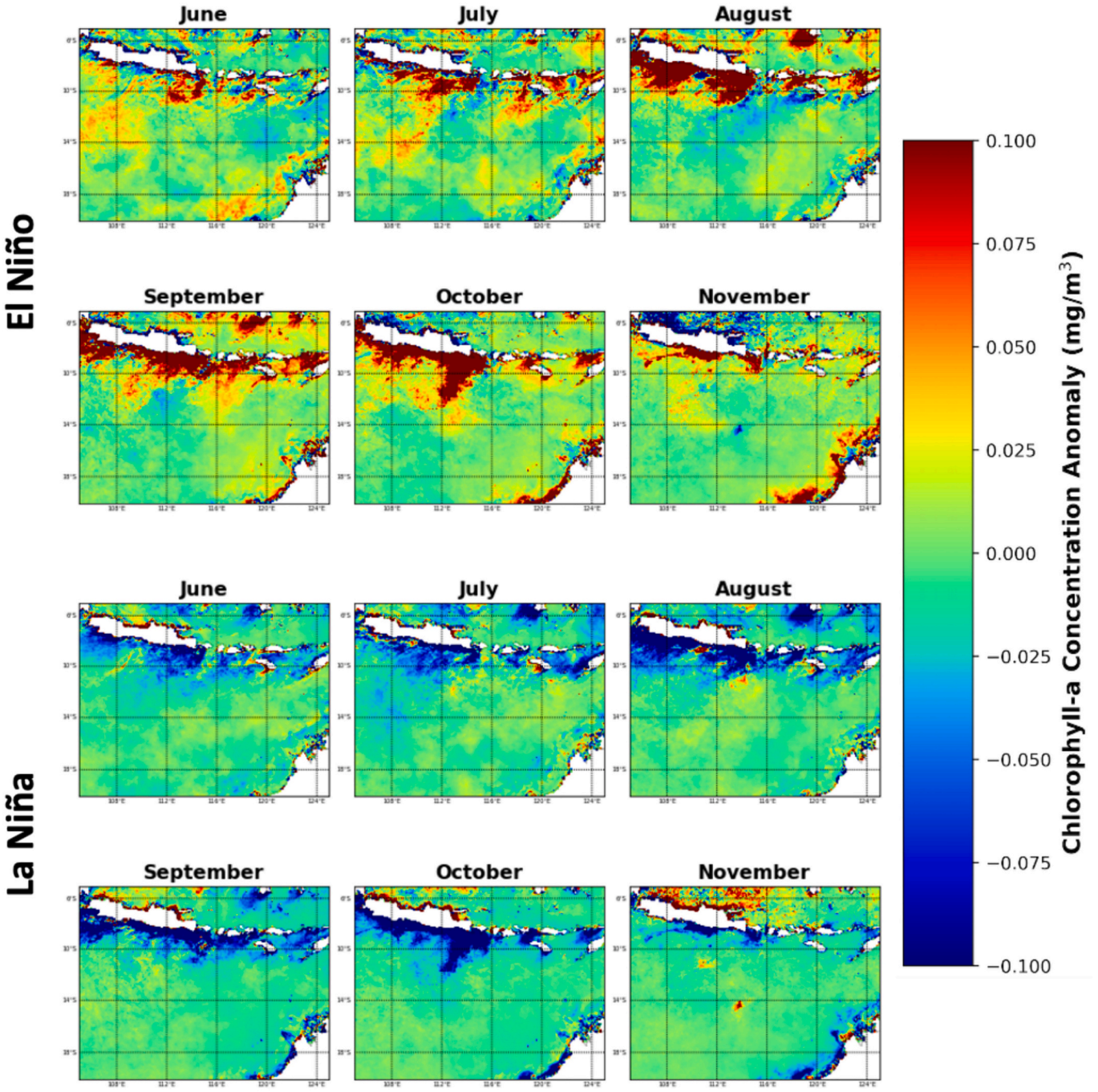

Fig. 10. Chlorophyll-a Anomaly during El Niño and La Niña.

IOD periods. The analysis results show that the windstress anomaly values exhibit different patterns between the El Niño/Positive IOD and La Niña/Negative IOD phenomena. During El Niño conditions, significantly high anomaly values occur from September to November, with a maximum reaching −0.01 N/m^2. This indicates that the westward windstress is relatively strong during these conditions. Conversely, during La Niña, the windstress tends to have positive values, reaching up to 0.01 N/m^2. Next, during IOD events, a similar pattern is observed. In Positive IOD, negative anomalies in zonal windstress occur from July to November. The magnitude of the negative anomaly during Positive IOD tends to be greater compared to El Niño conditions, with a maximum reach of 0.18 N/m^2. During Negative IOD phases, the pattern is similar to La Niña, where negative windstress anomalies also occur in the SI region, with a maximum reaching 0.015 N/m^2.

As is known, the upwelling phenomenon that predominantly occurs in Indonesia is largely influenced by the movement of the SEM. The significantly high westward zonal windstress anomaly indicates that the energy required to generate upwelling is higher under these conditions. This means that during El Niño/IOD conditions, the windstress tends to be stronger towards the west, leading to increased interaction with the water masses, resulting in higher upwelling intensity. This is also shown by the analysis results of Ekman Pumping Velocity (EPV) calculations, which also indicate an increase under these conditions (Supplementary materials Fig. S2). Conversely, during La Niña/Negative IOD conditions, the positive anomaly value indicates that the zonal windstress is greater from west to east. This results in a decrease in upwelling intensity in the SI region.

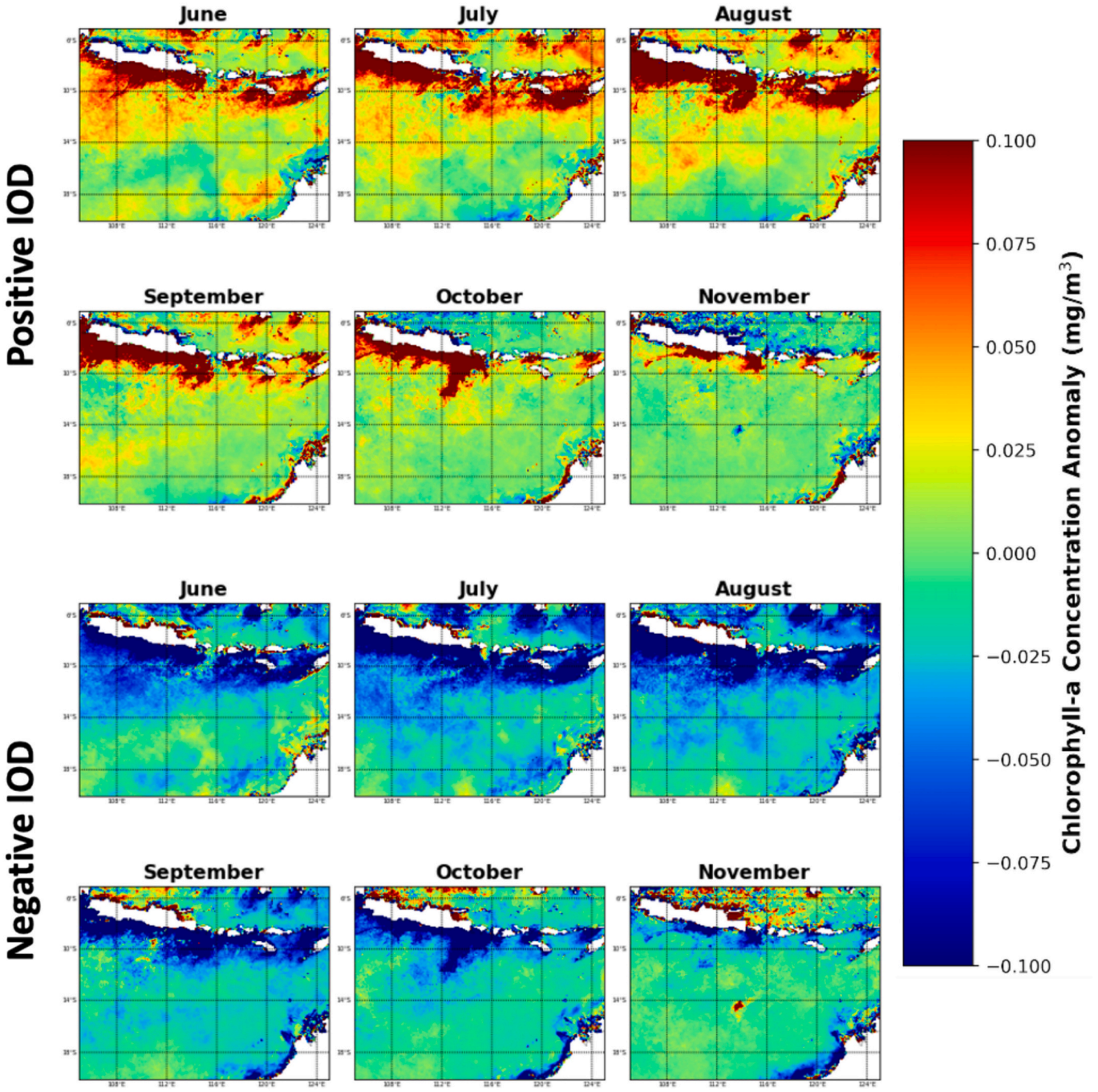

Fig. 11. Chlorophyll-a Anomaly during Positive IOD and Negative IOD.

4. Discussion

This research aimed to investigate the dynamic of upwelling phenomena in the Southern Indonesia (SI) region and its role in the ENSO and IOD phenomena. Generally, the upwelling phenomena along South Java and Nusa Tenggara occur from June to November, controlled by the Southeast Monsoon (SEM) wind (Susanto et al., 2006). Based the monthly analysis of SST chlorophyll-a concentration, and zonal wind-stress shows a changing pattern both in spatial and temporal distribution. This pattern was consistent with the Upwelling Indices (UI_{sst}) annual cycle calculated by the gradient from coastal and ocean locations. The wind movement during SEM (Supplementary materials Fig. S1) forms the current pattern that is perpendicular to the shoreline and causes the water masses movement from near the coast to the ocean area (far from the coast) (Santos et al., 2012; Varela et al., 2018). This condition makes the water mass void on the coast and replaces it with water mass from deep waters (Wyrtki, 1962). Based on analysis, data show that the strong intensity of upwelling in the SI region is mainly caused by the movement of southeast monsoon winds in the eastern season (June–November) (Varela et al., 2016; Wyrtki, 1962). The Hovmoller diagram pattern of UI_{sst} also shows the westward propagation of upwelling intensity. From April to June, high upwelling intensity developed on the southern coast of Flores and Sumbawa islands, and then from July to October, it peaks on the southern coast of East Java. The monthly averages of chlorophyll-a concentrations show an increase in the South of Sumbawa and Flores from May to June (Fig. 3). Meanwhile, it began to develop in the South of Java from July to September. The same pattern was also found based on previous results of the SST

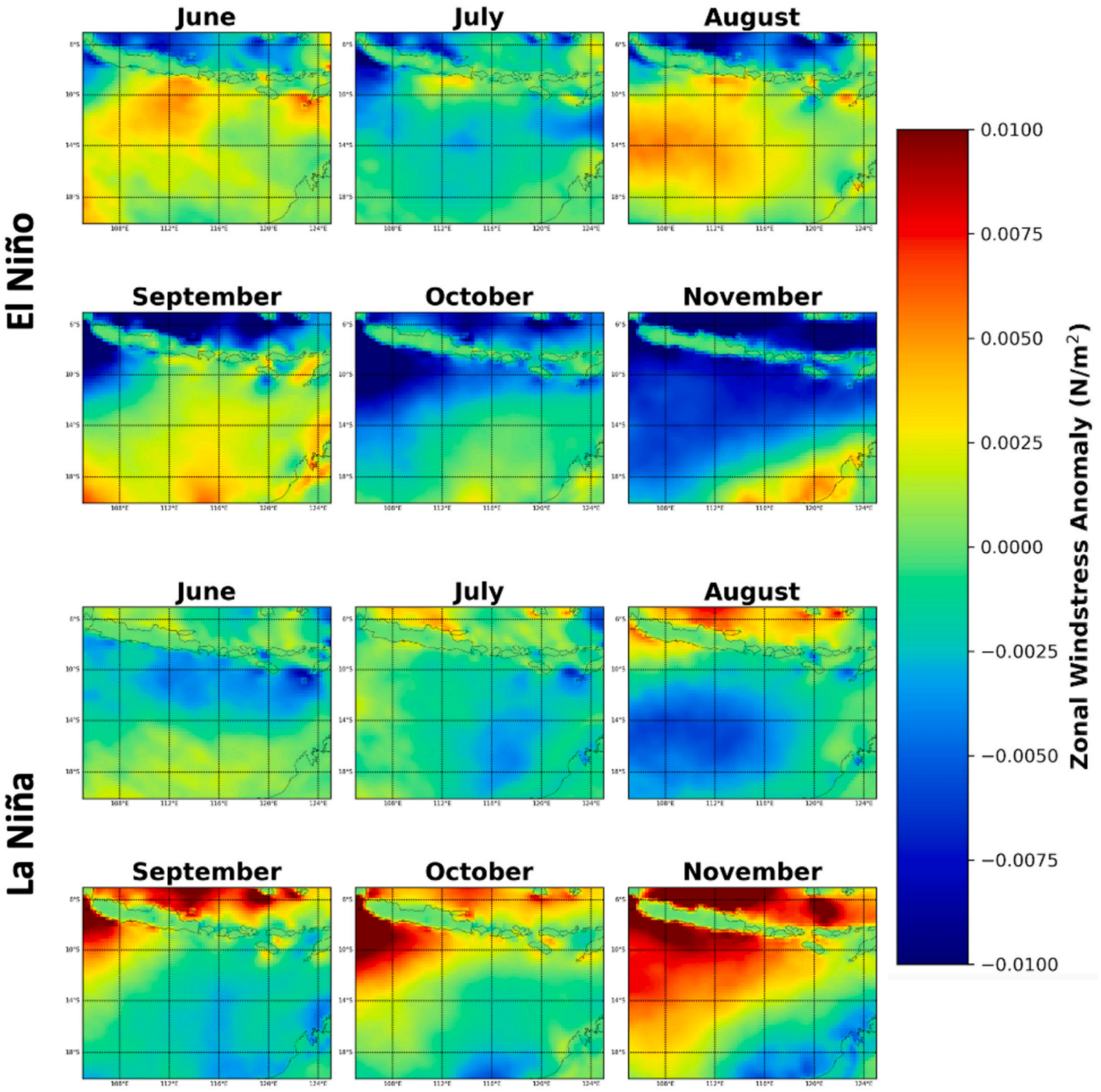

Fig. 12. Zonal Windstress anomaly during El Niño and La Niña.

propagation (Susanto et al., 2006) and Ekman Transport by (Wirasatriya et al., 2020).

The results showed a noteworthy finding in two sites (116–118°E and 122–124°E) (Fig. 5), where the UI_{sst} was less than in other areas. These sites are the ITF outlets in the Lombok and Ombai Strait. Based on General Circulation Models (GCMs), it has been hypothesized that the advection of warm pool water from the North Pacific by the ITF influences the SST in the Indonesian Seas, including in the study areas (Gordon and Fine, 1996; Susanto et al., 2006). Also, the recorded transport of the ITF is lowest during NWM and highest during SEM (Meyers et al., 1995). Therefore, a warmer and colder SST will probably occur in SEM and NWM from the seasonal SST variability caused by the ITF. Furthermore, the transport of the ITF is reported to have a maximum at the subsurface but not at the surface (Gordon et al., 2003). Moreover, heat advection from other closest seas, such as the South China Sea (Qu et al., 2006) and the South Pacific could impact SST (Qu et al., 2005). Yet, their transport is much smaller than the ITF and unlikely to significantly impact SST across the Indonesian Seas. As a consequence, this advection weakens the UIsst based on the SST gradient at the outlet location of the ITF in the SI region (Lombok Strait and Sabu Sea) (Figs. 2 and 5). This result is also in line with the research findings of (Kida and Richards, 2009)Also, the weakening of UI_{sst} is probably due to the warm water flow that causes the thermocline layer to become deeper. Consequently, the water layer with higher nutrients is unlikely to rise to the surface when the upwelling phenomenon occurs. The weakening of UI_{sst} in the outflow part of the ITF is also indicated by a decrease in chlorophyll-a concentrations, especially in the southern part of the Lombok Strait and Sabu Sea (Fig. 3).

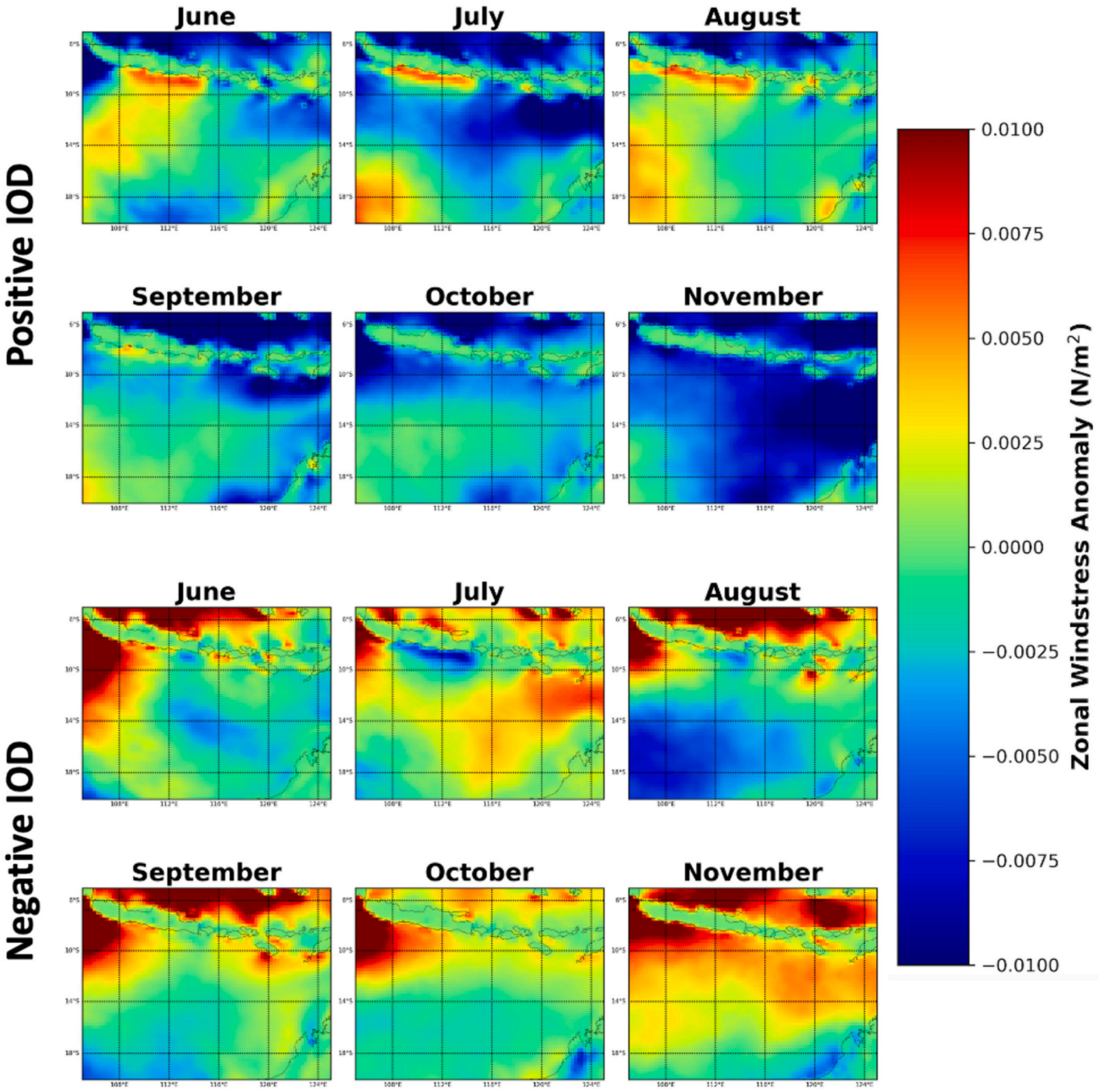

Fig. 13. Zonal Windstress anomaly during Positive IOD and Negative IOD.

Furthermore, the weakening UI_{sst} in the aforementioned location was clearly shown during extreme events such as Positive IOD (Fig. 7). This weakening index may be due to the low wind stress anomaly, as shown in Figs. 12 and 13. According to Atmadipoera et al. (2020), wind stress, and upwelling intensity are correlated. However, previous research conducted by Wen et al. (2023), revealed that it's likely that wind stress has a minimal impact on the interannual variability of upwelling along the coast of South Java. Therefore, we calculated the ensemble monthly mean of the EPV (Supplementary materials Fig. S2), whereas the result revealed that the highest downward EPV occurred from May to October (SEM). This result also aligns with Wirasatriya et al. (2020) which stated that EPV along the South Java Coast is stronger in SEM than in NWM. Also, the strong upwelling intensity along the SI region occurred during the SEM. The strong southeasterly winds (Figs. 12 and 13) and the wind curl will generate the downward EPV (Supplementary materials Fig. S2), which triggers coastal upwelling. However, the UI_{sst} trend is inconsistent with the spatial distribution of EPV (Supplementary materials Fig. S2), and this inconsistency was also found in Wen et al. (2023). Another research by Chen et al. (2016) revealed that interannual variations in SST are significantly influenced by interannual variability in the local wind pattern. This situation also suggests that UI_{sst} is a more effective indicator of upwelling in the study area, which aligns with the findings of previous research by Budiman et al. (2022).

A partial correlation analysis examined UI's$_{sst}$ interannual variability in the SI region. These two phenomena strongly influence the intensity of upwelling in the SI region. By using partial correlation analysis, it shows that the influence of IOD tends to be greater than ENSO,

particularly in the western side of the SI region. A high correlation between UI_{sst} and IOD occurs during the peak period of the Upwelling phenomenon from June to October, especially in the upwelling hotspot ($UI_{sst} \geq 0.9\ ^{\circ}C$) during August on the western side. The positive (negative) IOD phenomenon causes a decrease (increase) in the SST around the Eastern Indian Ocean (EIO), where the SI region is also included. It is known that the IOD event peaks in the October–November period each year of its occurrence (Saji et al., 1999). In Positive IOD conditions, the decrease in SST also causes a shallower depth of the thermocline layer (Shi and Wang, 2024). Therefore, the upper layer of water will be more easily mixed, increasing the UI_{sst}. During Negative IOD, the EIO region tends to be warmer than normal, which causes the thermocline layer to become shallower. As a result, the intensity of upwelling tends to be higher than normal conditions (Fig. 6). As for the ENSO phenomenon, the correlation analysis results show that the maximum correlation value occurs in August–November. However, after the influence of IOD is removed using partial correlation, it is evident that the actual influence of ENSO on UI_{sst} in the western region only occurs in November. The magnitude of the correlation analysis, both partially/non-partially, still tends to be lower than the IOD. Generally, the influence of ENSO on UI_{sst} appears weaker compared to IOD, particularly in the western hotspot region of UI_{sst}, while the eastern hotspot is influenced by both phenomena. The weakness of ENSO's influence is likely due to the time lag of ENSO's effect on UI_{sst} in the SI region, which reaches 2 months, with the peak of UI_{sst} occurring 2 months earlier than the peak of ENSO. In contrast, the influence of IOD on UI_{sst} does not have a time lag (Supplementary materials Fig. S3). In this region, the influence of ENSO and IOD on UI_{sst} is relatively similar to the influence of both phenomena on SST as reported by Hendon (2003) and As-syakur Abd et al. (2014), which suggests the consistency of this analysis.

The response of increased UI_{sst} during extreme conditions can be observed in SST and chlorophyll-a, anomalies with a harmonious pattern. During El Niño/Positive IOD, SST anomaly will tend to be lower, and chlorophyll-a anomaly will be higher than normal. The opposite condition occurs when La Niña/Negative IOD. The low SST value during El Niño/Negative IOD is closely related to the strength of upwelling in the SI region. The results of previous studies also show that SST conditions have a fairly strong correlation to these two phenomena, especially during the June–November period or during the SEM period (As-syakur Abd et al., 2014). The difference in magnitude between the SST and chlorophyll-a anomaly readings indicates that the IOD phenomena are more significant than ENSO. The mature phase of IOD development in the waters off southern Indonesia peaks in June to August. This is confirmed by Saji et al. (1999), who report that IOD starts to exhibit an increase in the significance of SST anomalies in the EIO region during the May–June period and that this rise peaks in October. This is believed to contribute to the upwelling intensification shown in Figs. 7 and 10, which both show that the peak of the IOD effect happens between June and October. However, according to the SST Anomaly distribution map, the largest value in the IOD occurs in June (Fig. 10). The temporary assumption is that El Niño and La Niña's influence in the SI region peaks between September and October. As-syakur Abd et al. (2014) also described the findings of this investigation, which found that ENSO had a peak influence in the southern region of Indonesia from September to November.

This study emphasized interannual scales, whereas ENSO and the IOD dominate the variability. However, the upwelling at different timescales, such as intraseasonal and mesoscales eddies, seems significant (Vinayachandran et al., 2002). A prior investigation demonstrates the function of two eddies in the distribution of the upwelling filament (i.e., contains heat, chlorophyll-a) and water during cross-shelf transport in the South of Java (Ismail et al., 2024). This phenomenon can be explained by a triple chain of mechanisms: the intensification of coastal nutrients by wind-driven upwelling, persistence, and offshore export by the frontal cyclonic eddy onshore and the advection farther south by the anticyclonic eddy offshore (Ismail et al., 2024). Therefore, the combined effect of enhanced coastal upwelling caused by southeasterly winds and two eddies' propagation and retention abilities may provide reasons for nutrient-rich coastal waters in offshore areas. Moreover, the strong south Java currents and mesoscale cyclonic eddies resulted in large surface chlorophyll-a blooms and upwelling during SEM triggered by seasonal Ekman mass transport (Mandal et al., 2022). A previous study also states a clear correlation between high eddy kinetic energy and offshore chlorophyll-a blooms in the southeastern tropical Indian Ocean, especially south of Java during boreal summer-fall 2006 (Iskandar et al., 2010). Yet, the upwelling along the Sumatra-Java shores is primarily triggered by alongshore winds during the SEM and is highly affected by IOD events (Vinayachandran et al., 2021); we only limit our upwelling analysis to SST, chlorophyll-a, and wind stress.

However, this study still has some uncertainties. This study only focused on how long-term satellite datasets of SST provide consistent information on upwelling phenomena related to ENSO and IOD from 1982 to 2022 along the SI region. Also, we focused on how the relationship between the simplified UI_{sst} index and ENSO and IOD. This long-term record can be used for further applicable information, such as estimating the impact of local fisheries' resources due to climate variability. Therefore, we had a limitation analysis related to wind stress, Ekman Transport, and the Ekman Pumping process, which may also trigger the upwelling intensity within the region. Although we have carried out the analysis, it is not the primary focus of this study; therefore, a more comprehensive analysis will be necessary in the future. Meanwhile, to enrich future studies, combining multiple upwelling indexes (i.e., UI_{sst} and UI from Winds and other UI's) is necessary, including estimating the contribution from the wind effects to the total upwelling intensity.

5. Conclusion

This study shows that chlorophyll-a and SST data from satellite data can provide an overview of the spatiotemporal pattern of upwelling intensity and its relationship with ENSO and IOD in the SI region. Based on UI_{sst} calculations, the upwelling pattern started in the April to May period from the southern part of Nusa Tenggara Islands and then propagated westward to the South Coast of Java. The UI_{sst} distribution pattern is also confirmed by the spatiotemporal pattern of chlorophyll-a, which propagates from east to west, and a declining pattern of UI_{sst} in the area became the outlet of the ITF, which was temporarily suspected due to the constant input of warmer water masses from the Pacific to the Indian Ocean. Correlation analysis was performed to examine the influence of interannual phenomena, in this context, ENSO and IOD, on upwelling intensity in SI. The result indicated from the partial correlation analysis that the western region of the study area is influenced by IOD from May to October, while November is influenced by ENSO. In contrast, the eastern region shows a more complex relationship between UI_{sst} and ENSO and IOD, where ENSO is affected in April–May, and IOD influences it from June to October. Finally, in general, the influence of IOD on UI_{sst} is stronger and wider compared to the influence of ENSO.

Funding

This work is partly funded by the European Space Agency - Future Earth Joint Program to the SKLEC, East China Normal University (project 'EO-WPI') and administered by IMBeR IPO-China.

CRediT authorship contribution statement

Herlambang Aulia Rachman: Writing – original draft, Methodology, Investigation, Formal analysis, Conceptualization. **Martiwi Diah Setiawati:** Writing – review & editing, Supervision, Conceptualization, Funding acquisition. **Zainul Hidayah:** Investigation. **Achmad Fachruddin Syah:** Writing – review & editing. **Muhammad Rizki Nandika:** Methodology, Investigation, Conceptualization. **Jonson Lumban-Gaol:**

Writing – review & editing. **Abd. Rahman As-syakur:** Writing – review & editing, Supervision, Data curation, Conceptualization. **Fadli Syamsudin:** Writing – review & editing.

Declaration of competing interest

The authors declare that they have no known competing financial interests or personal relationships that could have appeared to influence the work reported in this paper.

Declaration of Generative AI and AI-assisted technologies in the writing process

During the preparation of this work the author(s) used [Grammarly] to [improve the language and readability]. After using this tool/service, the author(s) reviewed and edited the content as needed and take(s) full responsibility for the publication's content.

Data availability

Data will be made available on request.

Appendix A. Supplementary data

Supplementary data to this article can be found online at https://doi.org/10.1016/j.seares.2024.102543.

References

Ashok, K., Behera, S.K., Rao, S.A., Weng, H., 2007. El Nin˜o Modoki and its possible teleconnection. J. Geophys. Res. 112, 1–27. https://doi.org/10.1029/2006JC003798.

As-syakur Abd, R., Adnyana, I.W.S., Mahendra, M.S., Arthana, I.W., Merit, I.N., Kasa, I. W., Ekayanti, N.W., Nuarsa, I.W., Sunarta, I.N., 2014. Observation of spatial pattern on the rainfall response to ENSO and IOD over Indonesia using TRMM multisatellite precipitation analysis (TMPA). Int. J. Climatol. 34, 3825–3839.

Atmadipoera, A.S., Jasmine, A.S., Purba, M., Kuswardani, A.R.T.D., 2020. Upwelling characteristics in the southern Java waters during strong La Niña 2010 and super El Niño 2015. Jurnal Ilmu Dan Teknologi Kelautan Tropis 12 (1), 257–276.

Benazzouz, A., Mordane, S., Orbi, A., Chagdali, M., Hilmi, K., Atillah, A., Pelegri, J.L., Demarq, H., 2014. An improved coastal upwelling index from sea surface temperature using satellite-based approach – the case of the canary current upwelling system. Cont. Shelf Res. 81, 38–54. https://doi.org/10.1016/j.csr.2014.03.012.

Blair, T.A., 1918. Partial correlation applied to Dakota data on weather and wheat yield. Mon. Weather Rev. 46 (2), 71–73.

Budiman, A.S., Bengen, D.G., Nurjaya, I.W., Arifin, Z., Ismail, M.F.A., 2022. A comparison of the three upwelling indices in the South Java Sea shelf. Chiang Mai University Journal of Natural Sciences 21 (3). https://doi.org/10.12982/CMUJNS.2022.044.

Chen, G., Han, W., Li, Y., Wang, D., 2016. Interannual variability of equatorial eastern Indian Ocean upwelling: local versus remote forcing. J. Phys. Oceanogr. 46 (3), 789–807.

Gordon, A.L., Fine, R.A., 1996. Pathways of water between the Pasific and Indian oceans in the Indonesian seas. Nature 376 (6561), 146–149.

Gordon, A.L., Susanto, R.D., Vranes, K., 2003. Cool Indonesian throughflow as a consequence of restricted surface layer flow. Nature 425 (6960), 824–828.

Hein, H., Hein, B., Pohlmann, T., Long, B.H., 2013. Inter-annual variability of upwelling off the south-Vietnamese coast and its relation to nutrient dynamics. Glob. Planet. Chang. 110, 170–182. https://doi.org/10.1016/j.gloplacha.2013.09.009.

Hendon, H.H., 2003. Indonesian rainfall variability : impacts of ENSO and local air – sea interaction. J. Clim. 16 (11), 1775–1790.

Hood, R.R., Beckley, L.E., Wiggert, J.D., 2017. Biogeochemical and ecological impacts of boundary currents in the Indian Ocean. Prog Oceanogr. 156, 290–325. https://doi.org/10.1016/j.pocean.2017.04.011.

Horhoruw, S.M., Atmadipoera, A.S., Nanlohy, P., Nurjaya, I.W., 2017. Anomaly of surface circulation and Ekman transport in Banda Sea during "Normal" and ENSO episode (2008-2011). IOP Conference Series: Earth and Environmental Science 54 (1), 012–041. https://doi.org/10.1088/1755-1315/54/1/012041.

Horii, T., Ueki, I., Ando, K., 2018. Coastal upwelling events along the southern coast of Java during the 2008 positive Indian Ocean dipole. J. Oceanogr. 74 (5), 499–508. https://doi.org/10.1007/s10872-018-0475-z.

Horii, T., Ueki, I., Siswanto, E., Iskandar, I., 2023. Long-term shift and recent early onset of chlorophyll-a bloom and coastal upwelling along the southern coast of Java. Frontiers in Climate 5. https://doi.org/10.3389/fclim.2023.1050790.

Iskandar, I., Sasaki, H., Sasai, Y., 2010. A numerical investigation of eddy-induced chlorophyll bloom in the A numerical investigation of eddy-induced chlorophyll bloom in the southeastern tropical Indian Ocean during Indian Ocean dipole — 2006. Ocean Dyn. 60 (June), 731–742. https://doi.org/10.1007/s10236-010-0290-6.

Ismail, M.F.A., Budiman, A.S., Basit, A., Yulihastin, E., Sofiati, I., Mujiasih, S., 2024. Cross-shelf transport of high chlorophyll-a coastal waters by frontal eddies in the south of Java Sea. Kuwait Journal of Science 51 (4). https://doi.org/10.1016/j.kjs.2024.100253.

Jacox, M.G., Edwards, C.A., Hazen, E.L., Bograd, S.J., 2018. Coastal upwelling revisited: Ekman, Bakun, and improved upwelling indices for the U.S. west coast. J. Geophys. Res. Oceans 123 (10), 7332–7350. https://doi.org/10.1029/2018JC014187.

Jayaram, C., Jose, F., 2022. Relative dominance of wind stress curl and Ekman transport on coastal upwelling during summer monsoon in the southeastern Arabian Sea. Cont. Shelf Res. 244 https://doi.org/10.1016/j.csr.2022.104782.

Juneng, L., Tangang, F.T., 2005. Evolution of ENSO-related rainfall anomalies in Southeast Asia region and its relationship with atmosphere - ocean variations in indo-Pacific sector. Clim. Dyn. 25 (4), 337–350. https://doi.org/10.1007/s00382-005-0031-6.

Kida, S., Richards, K.J., 2009. Seasonal Sea surface temperature variability in the Indonesian seas. J. Geophys. Res. Oceans 114 (C6).

Lumban-Gaol, J., Leben, R.R., Vignudelli, S., Okada, Y., Nababan, B., Mei-ling, M., Arhatin, R.E., Syahdan, M., 2015. Variability of satellite-derived sea surface height anomaly, and its relationship with Bigeye tuna (*Thunnus obesus*) catch in the Eastern Indian Ocean. European Journal of Remote Sensing 48 (1), 465–477. https://doi.org/10.5721/EuJRS20154826.

Lumban-Gaol, J., Siswanto, E., Mahapatra, K., Natih, N.M.N., Nurjaya, I.W., Hartanto, M. T., Maulana, E., Adrianto, L., Rachman, H.A., Osawa, T., Rahman, B.M.K., Permana, A., 2021. Impact of the strong downwelling (upwelling) on small pelagic fish production during the 2016 (2019) negative (positive) indian ocean dipole events in the eastern indian ocean off java. Climate 9 (2), 1–11. https://doi.org/10.3390/cli9020029.

Mandal, S., Susanto, R.D., Ramakrishnan, B., 2022. On investigating the dynamical factors modulating surface chlorophyll-a variability along the South Java coast. Remote Sens. 14 (7), 1745.

Meyers, G., Bailey, R.J., Worby, A.P., 1995. Geostrophic transport of Indonesian throughflow. Deep-Sea Res. I Oceanogr. Res. Pap. 42 (7), 1163–1174.

Ningsih, N.S., Rakhmaputeri, N., Harto, A.B., 2013. Upwelling variability along the southern coast of Bali and in Nusa Tenggara waters. Ocean Science Journal 48 (1), 49–57. https://doi.org/10.1007/s12601-013-0004-3.

Nugroho, S.C., Setiawan, R.Y., Setiawati, M.D., Djumanto, Priyono, S. B., Susanto, R. D., Wirasatriya, A., & Larasati, R. F., 2023. Estimation of albacore tuna potential fishing grounds in the southeastern Indian Ocean. IEEE Access 11, 1141–1147. https://doi.org/10.1109/ACCESS.2022.3233353.

Purba, N.P., Khan, A.M.A., 2019. Upwelling session in Indonesia waters. World News of Natural Sciences 25.

Qu, T., Du, Y., Strachan, J., Meyers, G., Slingo, J., 2005. Sea Surface Temperatureand Its Variability. Oceanography 18 (4), 50.

Qu, T., Du, Y., Sasaki, H., 2006. South China Sea throughflow: A heat and freshwater conveyor. Geophys. Res. Lett. 33 (23).

Rachman, H.A., Lumban-Gaol, J., Syamsudin, F., 2020. Remote Sensing of Coastal Upwelling Dynamics in the Eastern Indian Ocean off Java, Role of ENSO and IOD. In: Proceeding - AGERS 2020: IEEE Asia-Pacific Conference on Geoscience, Electronics and Remote Sensing Technology: Understanding the Interaction of Land, Ocean and Atmosphere: Disaster Mitigation and Regional Resillience, pp. 30–35. https://doi.org/10.1109/AGERS51788.2020.9452779.

Reynolds, R.W., 2009. What's New in Version 2, pp. 1–10.

Sahri, A., Herwata Putra, M.I., Kusuma Mustika, P.L., Kreb, D., Murk, A.J., 2021. Cetacean habitat modelling to inform conservation management, marine spatial planning, and as a basis for anthropogenic threat mitigation in Indonesia. Ocean Coast. Manag. 205 https://doi.org/10.1016/j.ocecoaman.2021.105555.

Saji, N.H., Goswani, B.N., Vinayachandran, P.N., Yamagata, T., 1999. A dipole mode in the tropical Indian Ocean. Nature 401 (September), 360–364.

Sambah, A.B., Iranawati, F., Julindasari, S.H., Pranoto, D., Harlyan, L.I., Ghafiky, A.F., 2017. The spatial analysis in tuna habitat related to the ocean variability in the Indian Ocean. http://oceancolor.gsfc.nasa.gov/.

Santos, F., DeCastro, M., Gómez-Gesteira, M., Álvarez, I., 2012. Differences in coastal and oceanic SST warming rates along the canary upwelling ecosystem from 1982 to 2010. Cont. Shelf Res. 47, 1–6. https://doi.org/10.1016/j.csr.2012.07.023.

Setiawan, R.Y., Wirasatriya, A., Hernawan, U., Leung, S., Iskandar, I., Wirasatriya, A., Hernawan, U., Leung, S., Iskandar, I., 2019. Spatio-temporal variability of surface chlorophyll-a in the Halmahera Sea and its relation to ENSO and the Indian Ocean dipole. Int. J. Remote Sens. 00 (00), 1–16. https://doi.org/10.1080/01431161.2019.1641244.

Setiawati, M.D., Sambah, A.B., Miura, F., Tanaka, T., As-Syakur, A.R., 2015. Characterization of bigeye tuna habitat in the southern waters off Java-Bali using remote sensing data. Adv. Space Res. 55 (2), 732–746. https://doi.org/10.1016/j.asr.2014.10.007.

Setiawati, M.D., Rachman, H.A., As-syakur, A.R., Setiawan, R.Y., Syahailatua, A., Wouthuyzen, S., 2024. The habitat preference of commercial tuna species based on a daily environmental database approach in the tropical region of the eastern Indian Ocean off Java-Bali waters. Deep-Sea Research Part II: Topical Studies in Oceanography 216. https://doi.org/10.1016/j.dsr2.2024.105400.

Shi, W., Wang, M., 2024. Ocean variability in the Costa Rica thermal dome region from 2012 to 2021. Remote Sens. 16 (8), 1340.

Siswanto, Suratno, 2005. Seasonal pattern of wind induced upwelling over Java – Bali Sea. International Journal of Remote Sensing and Earth Sciences (IJReSES) 5, 1–8.

Sprintall, J., Chong, J., Syamsudin, F., Morawitz, W., Hautala, S., Bray, N., Wijffels, S., 1999. Dynamics of the South Java current in the indo-Australian Basin. Geophys. Res. Lett. 26 (16), 2493–2496.

Susanto, R.D., Marra, J., 2005. Effect of the 1997/1998 El Nino on along the southern coasts of Java and Sumatra. Oceanography 18 (4), 124–127.
Susanto, R.D., Gordon, A.L., Zheng, Q., 2001. Upwelling along the coasts of Java and Sumatra and its relation to ENSO. Geophys. Res. Lett. 28 (8), 1599–1602. https://doi.org/10.1029/2000GL011844.
Susanto, R.D., Moore, T.S., Marra, J., 2006. Ocean color variability in the Indonesian seas during the SeaWiFS era. Geochem. Geophys. Geosyst. 7 (5), 1–16. https://doi.org/10.1029/2005GC001009.
Syah, A.F., Lumban-Gaol, J., Zainuddin, M., Apriliya, N.R., Berlianty, D., Mahabror, D., 2019. Habitat model development of bigeye tuna (Thunnus obesus) during southeast monsoon in the eastern Indian Ocean using satellite remotely sensed data. IOP Conference Series: Earth and Environmental Science 276 (1). https://doi.org/10.1088/1755-1315/276/1/012011.
Syamsuddin, M., Saitoh, S.I., Hirawake, T., Syamsudin, F., Zainuddin, M., 2016. Interannual variation of bigeye tuna (Thunnus obesus) hotspots in the eastern Indian Ocean off Java. Int. J. Remote Sens. 37 (9), 2087–2100. https://doi.org/10.1080/01431161.2015.1136451.
Undap, M.W.B.W., Suryoputro, A.A.D., Wirasatriya, A., 2023. Strong negative Indian Ocean dipole phenomenon in 2016 reduce the upwelling intensity along the seas of southern Java. Ecological Engineering and Environmental Technology 24 (9), 84–95. https://doi.org/10.12912/27197050/172873.
Varela, R., Santos, F., Gómez-Gesteira, M., Álvarez, I., Costoya, X., Días, J.M., 2016. Influence of coastal upwelling on SST trends along the south coast of Java. PLoS One 11 (9), 1–14. https://doi.org/10.1371/journal.pone.0162122.
Varela, R., Costoya, X., Enriquez, C., Santos, F., 2018. Differences in coastal and oceanic SST trends north of Yucatan peninsula. J. Mar. Syst. 182, 46–55. https://doi.org/10.1016/j.jmarsys.2018.03.006.
Vinayachandran, P.N.M., Iizuka, S., Yamagata, T., 2002. Indian Ocean dipole mode events in an ocean general circulation model. Deep-Sea Res. II 49, 1573–1596.
Vinayachandran, P.N.M., Masumoto, Y., Roberts, M.J., Huggett, J.A., Halo, I., Chatterjee, A., Amol, P., Gupta, G.V.M., Singh, A., Mukherjee, A., Prakash, S., Beckley, L.E., Raes, E.J., Hood, R., 2021. Reviews and syntheses: Physical and biogeochemical processes associated with upwelling in the Indian Ocean. In: Biogeosciences (Vol. 18, Issue 22). Copernicus GmbH, pp. 5967–6029. https://doi.org/10.5194/bg-18-5967-2021.
Wahyudi, A.J., Triana, K., Masumoto, Y., Rachman, A., Firdaus, M.R., Iskandar, I., Meirinawati, H., 2023. Carbon and nutrient enrichment potential of South Java upwelling area as detected using hindcast biogeochemistry variables. Reg Stud Mar Sci 59, 102802. https://doi.org/10.1016/j.rsma.2022.102802.
Wen, C., Wang, Z., Wang, J., Li, H., Shi, X., Gao, W., Huang, H., 2023. Variation of the coastal upwelling off South Java and their impact on local fishery resources. J. Oceanol. Limnol. 41 (4), 1389–1404. https://doi.org/10.1007/s00343-022-2031-3.
Wirasatriya, A., Setiawan, J.D., Sugianto, D.N., Rosyadi, I.A., Haryadi, H., Winarso, G., Setiawan, R.Y., Susanto, R.D., 2020. Ekman dynamics variability along the southern coast of Java revealed by satellite data. Int. J. Remote Sens. 41 (21), 8475–8496. https://doi.org/10.1080/01431161.2020.1797215.
Wirasatriya, A., Susanto, R.D., Kunarso, K., Jalil, A.R., Ramdani, F., Puryajati, A.D., 2021. Northwest monsoon upwelling within the Indonesian seas northwest monsoon upwelling within the Indonesian seas. Int. J. Remote Sens. 42 (14), 5433–5454. https://doi.org/10.1080/01431161.2021.1918790.
Wyrtki, K., 1962. The upwelling in the region between Java and Australia during the south-east monsoon. Mar. Freshw. Res. 13 (3), 217–225.
Xu, T., Wei, Z., Li, S., Susanto, R.D., Radiarta, N., Yuan, C., Setiawan, A., Kuswardani, A., Agustiadi, T., Trenggono, M., 2021. Satellite-observed multi-scale variability of sea surface chlorophyll-a concentration along the south coast of the Sumatra-java islands. Remote Sens. 13 (14) https://doi.org/10.3390/rs13142817.
Yati, E., Sadiyah, L., Satria, F., Alabia, I.D., Sulma, S., Prayogo, T., Marpaung, S., Harsa, H., Kushardono, D., Lumban-Gaol, J., Budiarto, A., Efendi, D.S., Patmiarsih, S., 2024. Spatial distribution models for the four commercial tuna in the sea of maritime continent using multi-sensor remote sensing and maximum entropy. Mar. Environ. Res. 198 https://doi.org/10.1016/j.marenvres.2024.106540.